Per. Mineral. (2010), 79, 1, 27-55

doi: 10.2451/2010PM0002
http://go.to/permin

PERIODICO di MINERALOGIA
established in 1930

An International Journal of
MINERALOGY, CRYSTALLOGRAPHY, GEOCHEMISTRY, ORE DEPOSITS, PETROLOGY, VOLCANOLOGY
and applied topics on *Environment*, *Archeometry* and *Cultural Heritage*

Petrogenesis of the High-Alumina Basalt-Andesite suite from Sant'Antioco Island, SW Sardinia, Italy

Aida Maria Conte[1,*], Danilo Mauro Palladino[2], Cristina Perinelli[3] and Emmanuelle Argenti[4]

[1]C.N.R.- I.G.G.- U.O.S. di Roma, Dipartimento di Scienze della Terra, Sapienza Università di Roma, P.le Aldo Moro 5, 00185 Roma, Italy
[2]Dipartimento di Scienze della Terra, Sapienza Università di Roma, P.le Aldo Moro 5, 00185 Roma, Italy
[3]Dipartimento di Scienze della Terra, Università di Pisa, Via Santa Maria 53, 56126 Pisa, Italy
[4]Parco Naturale Regionale Bracciano Martignano, Via A. Saffi, 4/A, Bracciano, 00062 Roma, Italy

Submitted, November 2009 - Accepted, March 2010

Abstract - Present-day Sant'Antioco Island (SW-Sardinia, Italy) hosted one of the southernmost, and youngest, subduction-related, Cenozoic magmatic events of western Sardinia. A high-alumina basalt-andesite rock association, the focus of this paper, crops out in the southern portion of the island and represents the mafic end-member of volcanism developed during Miocene. Basaltic andesites and andesites are the dominant rock-types, while basalts and dacites are occasional. Minero-petrographic and geochemical characteristics reveal: *i*) a clear calc-alkaline signature for these rocks, in spite of high FeO*/MgO ratios that mimic a tholeiitic affinity; *ii*) a magma evolution mainly controlled by fractional crystallization and *iii*) some degree of crustal assimilation. Phase relationships and compositions, mass balance calculations and T, P, X_{H_2O} estimates consistently indicate that fractional crystallization occurred at low pressure (P=100-400 MPa), under different P_{H_2O} conditions, which explain the observed wide shifts in major oxides (e.g., Al_2O_3 and MgO), for comparable SiO_2 contents, and the ambiguous tholeiitic character as well. Phase relationships in the least evolved lithotypes point out that higher H_2O concentrations (estimated at up to 6 wt%) in the melts reduced the crystallization of plagioclase and favoured that of olivine, whereas lower H_2O contents (up to 3 wt%) promoted plagioclase fractionation and earlier crystallization of orthopyroxene at the expense of olivine. This X_{H_2O} imprint was recorded up to the most evolved compositions. Finally, the study rock suite can be derived from a parental (near-primary) magma matching in composition high-MgO basalts from the Montresta calc-alkaline district in NW Sardinia, in the light of the close compositional similarity between the high-Al_2O_3 basaltic andesites in the two districts. Thus, starting from a common parental composition, here we reconstruct liquid lines of descent, where the relative proportions of fractionating plagioclase *vs* mafic phases, as controlled by X_{H_2O} in the melts, may account for the compositional differences of Sant'Antioco rock-types *ab initio*.

Riassunto - L'Isola di Sant'Antioco (Sardegna sud-occidentale) ospita una delle più recenti manifestazioni del magmatismo orogenico del margine occidentale della Sardegna connesso alla subduzione cenozoica. Oggetto del presente lavoro sono le vulcaniti affioranti nella porzione meridionale dell'isola, costituite essenzialmente da andesiti basaltiche alte in allumina e da andesiti (più occasionali basalti e daciti), che rappresentano i termini meno differenziati del locale magmatismo di età miocenica. Oltre ad integrare l'ampio

* Corresponding author,
E-mail: aidamaria.conte@uniroma1.it

panorama degli studi esistenti sul magmatismo orogenico sardo, la caratterizzazione minero-petrografica e geochimica e la parametrizzazione P, T, X_{H_2O} dei litotipi investigati, consente una ricostruzione dei relativi processi petrogenetici, anche alla luce dei recenti sviluppi sperimentali sui sistemi calco-alcalini. I risultati indicano che le vulcaniti in esame rivelano una chiara affinità calco-alcalina, nonostante gli alti rapporti FeO*/MgO tipici di rocce di serie tholeiitica, e che la differenziazione magmatica è stata controllata principalmente dalla cristallizzazione frazionata, associata a differenti gradi di assimilazione crostale. Le relazioni di fase e i calcoli di bilancio di massa, in accordo con le stime di T e P di cristallizzazione dei fenocristalli e dei contenuti di H_2O in soluzione nei magmi, suggeriscono una cristallizzazione a bassa pressione (P=100-400 MPa) con differenti X_{H_2O}. Proprio quest'ultimo parametro spiega sia l'ampia variabilità composizionale di queste rocce (in particolare i differenti contenuti in Al_2O_3 e MgO per contenuti in SiO_2 simili), sia l'apparente carattere tholeiitico. Le relazioni di fase osservate nei litotipi meno evoluti indicano infatti che alte concentrazioni di H_2O nei fusi (stimate intorno al 6% in peso) hanno ridotto l'incidenza del plagioclasio (che tuttavia rappresenta invariabilmente la fase dominante, seguita dal clinopirosseno), favorendo la cristallizzazione dell'olivina fra le fasi femiche. Viceversa, minori contenuti in H_2O (fino a ~3%), oltre a favorire il frazionamento di plagioclasio, hanno comportato la precoce cristallizzazione dell'ortopirosseno a spese dell'olivina. L'evidenza di diversi contenuti in H_2O quale fattore di controllo determinante del processo di differenziazione dei magmi persiste fino alle composizioni più evolute dell'associazione in esame. Infine, le litologie meno differenziate riscontrate a Sant'Antioco possono essere considerate come direttamente derivanti da un magma più primitivo di composizione simile a quella dei basalti alti in MgO affioranti nel distretto vulcanico di Montresta (Sardegna nord-occidentale), anche sulla base delle significative analogie composizionali fra le andesiti basaltiche alte in Al_2O_3 nelle due aree. L'insieme dei dati è compatibile con un modello in cui, a partire da una comune composizione parentale, le differenze riscontrate sin dai termini meno evoluti di Sant'Antioco possono essere ricondotte a percorsi evolutivi caratterizzati da diversi rapporti tra le fasi frazionate (in particolare fra il plagioclasio e le fasi femiche) sotto il controllo cruciale della X_{H_2O}.

Key words: *Cenozoic orogenic volcanism, high-alumina basaltic-andesites, petrology and geochemistry, Sant'Antioco, Sardinia.*

Introduction

Cenozoic, subduction-related, igneous activity in Sardinia has been widely investigated (e.g., Dostal *et al.*, 1982; Beccaluva *et al.*, 1994; Brotzu *et al.*, 1997a, b; Morra *et al.*, 1994, 1997; Mattioli *et al.*, 2000; Downes *et al.*, 2001; Franciosi *et al.*, 2003; Lustrino *et al.*, 2004, 2009). However, information on petrography, mineralogy and chemistry of one of the southernmost volcanic districts, Sant'Antioco, is still scarce and incomplete. Up to now, the few geological and compositional data available on the Sant'Antioco volcanics were reported in Luxoro (1987), in the 1:25,000 geo-petrographic map of Sant'Antioco Island (Maccioni *et al.*, 1990) and in Lecca *et al.* (1997), who considered the andesitic *s.l.* rocks from Sant'Antioco Island as part of the orogenic magmatism in the Sulcis area (SW mainland Sardinia).

The Sulcis volcanic district is the southernmost part of the calc-alkaline magmatic belt that developed during late Eocene - middle Miocene time span (Lustrino *et al*., 2009) along the western side of Sardinia (Fig. 1), as a consequence of subduction acting in the Western Mediterranean Sea beneath the southern European margin (e.g., Doglioni, 1991; Doglioni *et al.*, 1999 and references therein).

This work illustrates the mineralogical, geochemical and petrological aspects of the Sant'Antioco volcanics in order to integrate the large set of studies on Cenozoic orogenic magmatism in Sardinia and to reconstruct petrogenetic processes. In particular, we focus on the influence of H_2O on the magma liquid lines of descent in the light of recent studies on natural and experimental calc-alkaline systems (Sisson and Grove, 1993a, b; Pichavant and Macdonald, 2007 and references therein; Ulmer, 2007 and

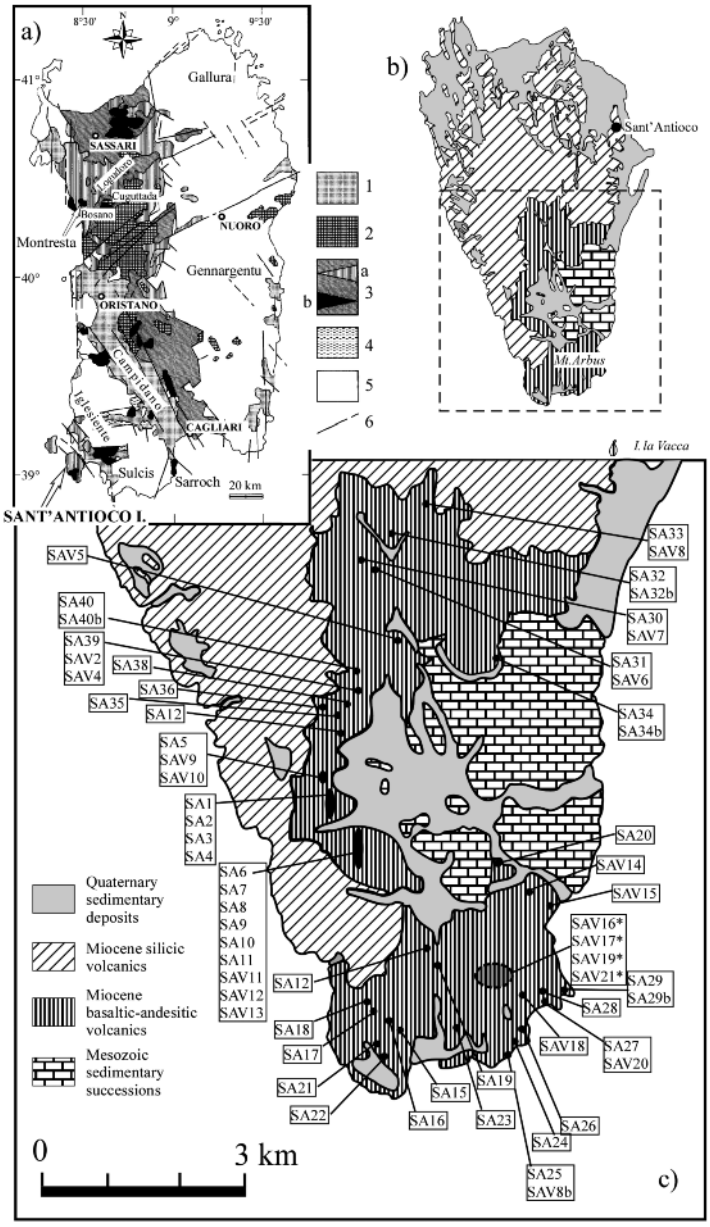

Fig. 1 - a) Geological sketch map of Sardinia, showing the location of Sant'Antioco Island and other subduction-related Cenozoic volcanics (after Cherchi and Montadert, 1982, Savelli *et al.*, 1979 and Morra *et al.*, 1997, modified). (1) Pliocene-Quaternary sediments; (2) Middle Miocene-Pleistocene anorogenic volcanics; (3) Late Eocene-Middle Miocene sedimentary and volcanic rocks: (3a) silicic ignimbrites; (3b) andesites *s.l.*; (4) continental sedimentary rocks of Cixerri Formation; (5) undifferentiated Paleozoic basement and Mesozoic up to Eocenic cover; (6) main Post-Paleozoic regional faults. b) Geological sketch map of Sant'Antioco Island. c) Enlargement of the area shown in b, where the sampling sites are reported. (* lava clasts in Pispisia-M.te Arbus polygenic breccias).

references therein). Furthermore, possible relationships with compositionally analogous, or even less differentiated, Cenozoic orogenic rock-types of western Sardinia will be considered, aiming at identifying a reliable near-primary parental magma for the studied rock association.

Geological background

The Sant'Antioco Island, located immediately offshore of southwestern mainland Sardinia (Italy; Fig. 1), extends 17.5 km in a N-S direction, with a maximum W-E width of 10 km. It is part of the calc-alkaline volcanic belt that stretches along the western coast of Sardinia, which developed during late Eocene-middle Miocene (38-12 Ma, Lustrino et al., 2009 and references therein) along the main branches of the "Sardinian Rift System" (Main Branch Volcanic Zone) and in Sulcis (South-Western Volcanic Zone; *sensu* Lecca *et al.*, 1997). The Sardinian Rift System and related magmatism are interpreted in the frame of the kinematic processes acting in the western Mediterranean, which involved the Hercynian paleo-margin of southern Europe. These processes occurred in connection with the back-arc spreading produced by the eastward roll-back of the westward-subducting plate related to convergence between Africa and Europe (Doglioni, 1991; Doglioni *et al.*, 1999 and references therein). This caused the separation and counterclockwise (i.e., southeastward) rotation of the Corsica-Sardinia continental microplate up to its present position (upper Oligocene-middle Miocene). In this context, the Cenozoic calc-alkaline magmatism of Sardinia is directly related to the subduction of oceanic crust. The earliest calc-alkaline magmatic events along the present western side of Sardinia predate the rotation of the Corsica-Sardinia microplate; then magmatism migrated southeastward following the west-directed, eastward retreating, subduction zone beneath Sardinia until middle Miocene. The Cenozoic orogenic magmas in Sardinia were emplaced through a variably thinned continental crust (ca. 30 to 20 km thick, from North to South; Egger *et al*., 1988; Sartori *et al*., 2004; Sau *et al.*, 2005), which may account for the differences in composition and eruptive style of magmatic activity from North to South along the Sardinian Rift (e.g., Lustrino *et al.*, 2002).

The Sulcis volcanic district, which includes a south-western coastal area of mainland Sardinia and the nearby islands of San Pietro and Sant'Antioco, represents the southernmost expression of orogenic magmatism in Sardinia (Fig. 1) and one of its youngest occurrences as well. Volcanic stratigraphy is characterized by: 1) lava and subordinate pyroclastic successions, including andesites, basaltic andesites and rare basalts, of Oligo-Miocene age, which crop out in Sulcis mainland (i.e., S. Giovanni Suergiu, Narcao, Giba) and in the southern part of Sant'Antioco, and 2) silicic welded ignimbrites and subordinate lava flows and domes, ranging in composition from dacites to comendites, of Miocene age, exposed in mainland Sulcis (Portoscuso area), in the northern and western parts of Sant'Antioco, and throughout the whole San Pietro Island (Assorgia *et al.*, 1990; Morra *et al.*, 1994; Pioli and Rosi, 2005; Pioli *et al.*, 2008).

The pre-volcanic substrate on Sant'Antioco includes biohermal-biostromal and oolitic limestones and silty marls of Cretaceous age, cropping out in the SE part of the island (Maccioni *et al.*, 1990). Almost all of the island is made up of volcanic rocks of Miocene age from both silicic, mainly explosive, and mafic to intermediate, mainly effusive, activities. Published K-Ar age data indicate values clustered at around 16-18 Ma (Araña *et al*., 1974; Savelli *et al.,* 1979; Montigny *et al.,* 1981; Maccioni *et al*., 1991). A younger age of about 12 Ma was recently obtained by $^{40}Ar/^{39}Ar$ determinations for the trachytic neck of Isola del Toro, South of Sant'Antioco (Lustrino et al., 2007), which is intermediate between the age of the last products

of the Oligo-Miocene orogenic igneous phase in SW Sardinia and the early volcanism of the late Miocene-Quaternary phase in SE Sardinia (ca. 6.64 Ma, Lustrino *et al.*, 2007).

Field characteristics of the studied rock-types

The present study investigates the mafic to intermediate volcanic rocks that crop out in the southern part of Sant'Antioco Island. These are represented by high- and low-aspect ratio lava flows and small lava domes (typically less than 1 km across), associated with minor pyroclastic deposits, locally cut by lava dykes. In order to characterize this volcanic activity on Sant'Antioco, a set of sixty-seven representative rock samples has been analyzed, as listed in Table 1 (sample localities are shown in Fig. 1). Table 1 also summarizes relevant field characteristics of the studied volcanics, along with their correlation with the units identified by previous studies (i.e., Luxoro, 1987; Maccioni *et al.*, 1990). Following the stratigraphic scheme of Luxoro (1987), the studied samples include: *i*) twenty-two samples from the "Lave iniziali" (early lavas, hereon abbreviated as LI), consisting of thick (up to 10 m), massive, lava

Table 1

List of the analyzed samples of Cenozoic mafic to intermediate volcanic rocks from Sant'Antioco Island studied in this work (sample locations in Fig. 1), grouped according to unit nomenclatures in Luxoro (1987) and Maccioni et al. (1990). LI: Lave iniziali (Early lavas); P: Pispisia-M.te Arbus polygenic volcanic breccias; LT: Lave terminali (Final lavas); F: lava dykes.

SAMPLES	FIELD ASPECT	Luxoro (1987)	Maccioni *et al*. (1990)
SA22, SA29-29b, SAV8b	Lava dyke	F	13a
SA21, SA24, SA25	Lava dyke	F	13b
SA1, SA2, SA3-3b, SA4, SA6, SA7, SA8, SA9, SA16, SA35, SA36, SA37, SA38, SA39, SA40-40b, SAV2, SAV4, SAV11, SAV12	Thin lava flow interbedded with scoriaceous levels	LT	14
SAV16, SAV17, SAV19, SAV21	Lava clasts in polygenic breccias	P	15a
SA19, SA27, SA28, SAV14, SAV15-15b, SAV20	Lava injections in polygenic breccias	P	15b
SA15-15b, SA23, SAV18	Thick lava flow or lava dome	LI	17a
SA5, SA10, SA11, SA30, SA34-34b, SAV7, SAV9, SAV10, SAV13	Thick lava flow	LI	18
SA12-12b, SA13, SA14, SA17, SA18, SA31, SA33, SAV5, SAV6, SAV8	Thick lava flow or lava dome	LI	19a
SA20, SA32-32b	Lava dome	LI	20

flows and lava domes; *ii*) eleven samples from lava injections and lava blocks within the Pispisia-M.te Arbus polygenic volcanic breccia deposits (hereon P); *iii*) twenty-seven samples from thin (usually 1.5 m-thick) lava flows, part of the "Lave terminali" (final lavas, hereon LT); *iv*) seven samples from lava dykes intersecting the above volcanics (hereon F).

Petrography

The studied Sant'Antioco volcanics range in composition from basalts to dacites (see Geochemistry section). Basaltic andesites largely prevail within LT rock-types, while andesites are dominant within LI lithologies. Both basaltic andesites and andesites occur in the Pispisia-M.te Arbus lava types (P), as well as in lava dykes (F). Hereafter, for the sake of simplicity, the products from P and F units are grouped within either the LI or LT main-types, on the basis of bulk rock composition and of common mafic phenocryst assemblages (plagioclase is invariably the main phase and opaques are ubiquitous, see below).

Lava rocks from both LI and LT mostly show porphyritic or glomeroporphyritic (15-48 vol% phenocrysts), isotropic to pilotaxitic or seriate, textures and microcrystalline groundmass. Phenocryst and groundmass assemblages, as determined from modal analyses in thin section, are reported in Table 2 for a set of representative samples.

LT rocks (also including part of F dykes) consist of basaltic andesites and occasional basalts characterized by the ubiquitous, although relatively scarce, presence of olivine (always <5 vol%) and by the prevalence of clinopyroxene (Cpx) on orthopyroxene (Opx). In a few cases, within the least evolved lavas, which show very low contents of mafic phenocrysts (about 5%), Opx is lacking and olivine (3-4 vol%) prevails on Cpx.

LI rocks (also including P lavas and part of F dykes) comprise basaltic andesites and occasional dacites characterized by: *i*) the ubiquitous presence of pyroxene phenocrysts, with Opx often prevailing on Cpx; *ii*) the lack or occasional presence of scarce amounts of olivine; *iii*) the occurrence of hornblende in two samples from the

Table 2

Modal analyses of the most representative LT and LI rock-types (at least 1000 points counted for each sample).

Rock-type	LT	LT	LT	LT	LI	LI	LI	LI
Sample:	SA7 HABA	SA40 HABA	SA35 HABA	SA3 HABA	SA12 AND	SA15 AND	SA31 AND	SA32 DAC
Plg (ph[a]+mph[b])	23.2	23.5	16.8	21.9	22.5	21.4	32.1	29.5
Ol (ph+mph)	3.5	5.4	3.5	0.2	-	-	-	-
Cpx (ph+mph)	6.6	4.2	0.6	9.1	0.6	2.5	3.4	2.7
Opx (ph+mph)	-	-	-	-	1.6	7.6	9.7	6.5
Opx mph	0.5	-	-	0.8	-	-	-	-
Fe-Ti oxides mph	1.0	1.1	0.9	1.5	1.3	2.3	2.5	1.9
Hbl ph	-	-	-	-	-	-	-	1.0
P.I. (ph+mph)	34.8	34.2	21.8	33.5	26.0	33.8	47.7	41.6
Gdm	65.2	66.8	78.2	66.5	74.0	66.2	52.3	58.4

[a] phenocrysts (> 0.5 mm); [b] microphenocrysts (> 0.05 mm); Plg: plagioclase; Ol: olivine; Cpx: clinopyroxene; Opx: orthopyroxene; Hbl: horneblende; P.I.: porphyritic index; Gdm: groundmass; HABA: high-Al_2O_3 basaltic andesite; AND: andesite; DAC: dacite.

most evolved andesites and in the dacite sample.

Phenocryst glomeri (mostly Cpx and Opx, associated with coarse-grained Fe-Ti oxides, subordinate plagioclase and occasional olivine) are more common in LI than LT and typically occur in two-pyroxene andesites (cfr. "Type a" microinclusions in Brotzu *et al.*, 1997a).

Mineral chemistry and geochemical features of whole rock samples are reported in the following sections. Analytical methods are illustrated in Appendix A.

Mineralogy

Plagioclase

Plagioclase is the most abundant phenocryst phase (up to 80% by volume of total phenocrysts and microphenocrysts) in both LT and LI groups. It usually occurs as individual, variably sized, euhedral grains or, mainly in andesites, in glomerocrystic aggregates. Plagioclase crystals often show continuous zoning and clear surfaces. Dusty or cellular textures may be present, where crystal portions may enclose glassy material. Plagioclase phenocrysts also enclose magnetite and minute plagioclase crystals or, more rarely, fine skeletal Cpx grains.

In LI rock-types, plagioclase crystals show common intracrystalline compositional ranges, with either normal (core: An_{75-67}; rim: An_{65-59}) or reverse (core: An_{64-68}; rim: An_{72-74}) zoning. Although usually normally zoned, LT plagioclases are characterized by a wider compositional pattern: phenocryst core compositions even $>An_{90}$ are observed in several examples, while phenocryst rim and microphenocryst mostly range An_{60-75} in composition (representative analyses are reported in Table 3). As a whole, the compositional ranges of LT plagioclase vary significantly, even within rocks with similar evolution degree. For example, if we consider the least evolved lithotypes, the prevailing plagioclase compositions vary from An_{75-85} (SA7), through An_{78-90} (SA40), to An_{85-93} (SA35) (Table 3; Fig. 2), concomitant with increasing Al_2O_3 contents in the corresponding whole rocks (cfr. Geochemistry section).

Pyroxenes

In LT rocks, Cpx is the dominant mafic phenocryst phase (5-15% by volume), while Opx usually does not exceed 5 vol%. With increasing degree of differentiation, the amount of Opx *vs* Cpx increases to become prevalent in most of the olivine-free LI samples. In these latter, Cpx and Opx phenocrysts are often associated in polycrystalline aggregates (glomeri). As a whole, Cpx may occur as: *i*) euhedral pheno- to microphenocryst grains; *ii*) coarser, rounded grains, sometimes enclosing corroded relics of olivine; *iii*) microgranular coronas that mantle both Opx and Cpx phenocrysts, mainly in evolved LI andesites; *iv*) microliths in the groundmass. Clinopyroxene is always augitic, with a narrow compositional range ($Wo_{37-45}\,En_{39-45}\,Fs_{11-20}$). No clear compositional variations are observed as a function of the degree of evolution from basalts to andesites: both Al_2O_3 (1.6-6.5 wt%) and TiO_2 (0.33-1.10 wt%) contents do not well correlate with the magnesium number [mg# = MgO/(MgO+FeO*) molar], as they show different amounts for comparable mg# values (e.g., LT in Fig. 3 and Table 4).

Orthopyroxene ($Wo_{2-4}\,En_{54-72}\,Fs_{25-42}$, Table 4) occurs as either euhedral to subhedral phenocrysts or microphenocrysts (either isolated or in polycrystalline glomeri), in some cases mantled by Cpx grains. Solid inclusions, commonly of magnetite and, more rarely, of plagioclase laths, are also found.

Olivine

Olivine mostly occurs in LT rocks and usually does not exceed 2-3 vol%. In a few, less evolved,

TABLE 3

Representative electron microprobe analyses of plagioclase from the Sant'Antioco study rock-types.

Unit	SA7 LT	SA7 LT	SA7 LT	SA7 LT	SA7 LT	SA7 LT	SA35 LT	SA35 LT	SA35 LT	SA35 LT	SA35 LT	SA35 LT	SA40 LT	SA40 LT	SA40 LT	SA40 LT	SA40 LT
	1/c	1/r	2/c	2/r	mph	g	1/c	1/r	2/c	3/c	mph	g	1/c	2/c	2/r	mph	g
SiO_2	45.45	48.78	47.43	47.54	47.73	48.99	44.89	49.64	43.61	45.89	46.44	49.21	44.42	45.50	47.65	46.82	47.86
Al_2O_3	34.88	31.26	33.05	32.92	32.38	31.65	34.05	31.19	35.92	34.68	33.30	31.92	35.55	31.74	32.97	33.71	32.59
FeO	0.84	0.63	0.85	0.64	0.90	0.76	0.54	0.97	0.62	0.64	0.81	0.93	0.58	0.66	0.61	0.67	0.83
CaO	17.77	16.18	16.62	15.85	15.70	14.97	19.70	15.73	19.25	17.87	16.91	14.99	18.68	17.71	15.80	16.83	15.57
Na_2O	1.56	2.88	2.19	2.73	2.77	3.27	0.87	3.03	0.74	1.53	2.18	3.25	1.14	1.71	2.87	2.21	2.86
K_2O	-	0.09	0.10	0.10	0.10	0.10	0.04	0.13	-	-	-	0.12	-	-	-	-	0.18
Total	*100.49*	*99.82*	*100.24*	*99.78*	*99.58*	*99.74*	*100.09*	*100.69*	*100.14*	*100.62*	*99.64*	*100.41*	*100.37*	*97.32*	*99.90*	*100.24*	*99.89*
An (mol %)	86.32	75.26	80.28	75.80	75.37	71.26	92.39	73.62	93.50	86.57	81.08	71.35	90.05	85.13	75.26	80.80	74.28
Ab (mol %)	13.68	24.24	19.14	23.63	24.06	28.17	7.38	25.66	6.50	13.43	18.92	27.99	9.95	14.87	24.74	19.20	24.69
Or (mol %)	0.00	0.50	0.58	0.57	0.57	0.57	0.22	0.72	0.00	0.00	0.00	0.66	0.00	0.00	0.00	0.00	1.02
K_D	2.40	1.18	1.59	1.22	1.19	0.96	5.12	1.17	5.88	2.63	1.75	1.04	4.12	2.60	1.38	1.91	1.37

Unit	SAV11 LT	SAV11 LT	SAV11 LT	SAV11 LT	SAV11 LT	SAV11 LT	SAV15 P	SAV15 P	SAV15 P	SAV15 P	SAV15 P	SAV5 LI	SAV5 LI	SAV5 LI	SAV5 LI	SAV5 LI	SAV5 LI
	1/c	1/r	2/c	2/r	mph	g	1/c	1/r	2/c	mph	g	1/c	1/r	2/c	2/r	mph	g
SiO_2	46.54	50.87	45.18	45.32	53.86	55.24	46.15	47.36	47.42	48.70	59.11	49.32	53.02	50.32	52.43	51.31	59.31
Al_2O_3	34.12	30.80	34.73	34.53	28.42	27.33	34.23	33.12	33.33	32.38	23.92	32.22	29.62	31.40	29.94	30.51	24.36
FeO	0.42	0.74	0.56	0.81	1.28	1.51	0.72	0.61	0.69	0.78	1.03	0.33	0.44	0.52	0.30	0.64	0.86
CaO	17.07	13.51	18.14	17.98	10.88	9.66	17.25	16.53	16.41	15.12	5.94	15.15	12.10	14.13	12.47	13.19	6.26
Na_2O	1.72	3.79	1.06	1.28	5.09	5.45	1.54	1.97	2.04	2.72	5.53	2.84	4.49	3.40	4.31	3.97	5.31
K_2O	-	-	-	-	0.29	0.72	-	-	0.13	-	3.66	-	0.22	0.13	0.20	-	3.88
Total	*99.87*	*99.71*	*99.67*	*99.92*	*99.82*	*99.91*	*99.89*	*99.59*	*100.02*	*99.70*	*99.19*	*99.86*	*99.89*	*99.90*	*99.65*	*99.62*	*99.98*
An (mol %)	84.58	66.33	90.44	88.59	53.24	47.40	86.09	82.26	81.01	75.44	29.25	74.67	59.06	69.14	60.81	64.74	30.55
Ab (mol %)	15.42	33.67	9.56	11.41	45.07	48.39	13.91	17.74	18.22	24.56	49.28	25.33	39.66	30.10	38.03	35.26	46.90
Or (mol %)	0.00	0.00	0.00	0.00	1.69	4.21	0.00	0.00	0.76	0.00	21.46	0.00	1.28	0.76	1.16	0.00	22.55
K_D	2.42	0.87	4.16	3.42	0.52	0.43	2.96	2.22	2.13	1.47	0.28	1.73	0.87	1.35	0.94	1.08	0.38

Note: c: phenocryst core; r: phenocryst rim (1, 2, 3: phenocryst identification); mph: microphenocryst; g: groundmass. The plagioclase-melt Ca-Na exchange distribution coefficients (K_D) are also reported (see text for calculation details).

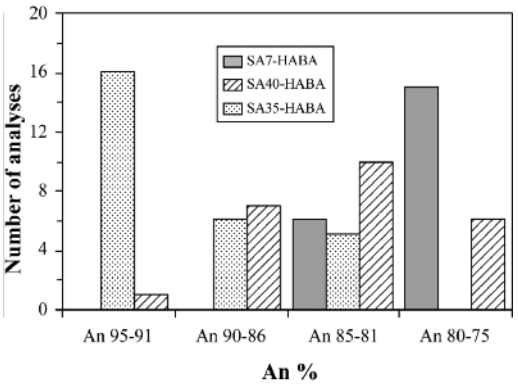

Fig. 2 - Frequency histograms displaying the variation of An contents in plagioclase of the SA7, SA35 and SA40 high-alumina basaltic andesite (HABA) samples from LT unit, which stand for the least evolved Sant'Antioco products (frequency expressed as number of analyses). Note that each sample shows a dominant plagioclase composition related to the Al_2O_3 content in the whole rock (cfr. TABLE 6).

rocks it may attain up to 5 vol% and represent the main mafic phase. Overall, Fo component ranges 50-59 mol%; individual crystals are usually normally zoned (TABLE 5). Generally, olivine crystals are altered to iddingsite, even if they preserve the original habit. In a few cases, fresh olivine relics are observed at the core of altered crystals. Some olivine crystals are bordered by granular Cpx.

Amphibole

Euhedral to subhedral amphibole phenocrysts, showing opacitic rims, are found in scarce amounts (<2 vol%) in two LI andesite samples with SiO_2 contents >58 wt% and in the dacite sample. Representative analyses, reported in TABLE 5, allow a classification as MgO-hornblende, following Leake *et al.* (2004). Compositional (i.e., low Al_2O_3 content, ~8 wt% on average) and textural relationships testify their late stage crystallization under low pressure conditions.

Fe-Ti oxides

Fe-Ti oxides (TABLE 5) are present ubiquitously both as microphenocrysts (either dispersed or bordering pyroxene phenocrysts) and, in higher amounts, as groundmass phases. Magnetite-titanomagnetite is common in basaltic andesites, while ilmenite only occurs in andesites.

GEOCHEMISTRY

Representative bulk rock compositions from the Sant'Antioco volcanics are reported in TABLE 6. Essentially they plot in the basaltic andesite and andesite fields of the TAS classification diagram (Le Bas *et al.*, 1986), with quite subordinate basalts and dacites. According to other classification diagrams, i.e. K_2O *vs* SiO_2 (Peccerillo and Taylor, 1976; Fig. 4a), and MgO *vs* Al_2O_3 (Kersting and Arculus, 1994; Fig. 4b), the studied products are mainly high-alumina basaltic andesites and andesites (with quite subordinate basalts and dacites: only one data point each) of medium-K calc-alkaline affinity. On the other hand, on the mere basis of the FeO*/MgO *vs* SiO_2 diagram (Miyashiro, 1974) all the investigated rocks would show a tholeiitic to mildly tholeiitic affinity (Fig. 4c). However, the plot of FeO*/MgO *vs* FeO* (inset in Fig. 4c) indicates that the relatively high values of FeO*/MgO in the Sant'Antioco rock suite are not accompanied by an iron enrichment trend typical of tholeiitic series. Furthermore, a possible tholeiitic affinity for the Sant'Antioco volcanics conflicts with the lack of pigeonite microphenocrysts (Kuno, 1959) and of Fe-enrichment in plagioclase (Aramaki and Katsura, 1973), as well as with the observed TiO_2 and Al_2O_3 contents, which pertain more properly to calc-alkaline rock-series. On these grounds, the relatively high FeO*/MgO ratios, which mimic a tholeiitic affinity, may be likely linked to the relative proportions of fractionating plagioclase

Table 4

Representative electron microprobe analyses of orthopyroxenes (a) and clinopyroxenes (b) from the Sant'Antioco study rock-types.

(a)	SAV12	SA7	SAV11	SAV11	SAV15	SAV15	SAV15	SAV15	SAV13	SAV13	SA10	SAV5	SAV5	SAV8	SAV8
Unit	LT	LT	LT	LT	P	P	P	P	LI	LI	LI	LI	LI	LI	LI
	r	c	c	r	c	r	mph	g	r	mph	c	c	r	c	r
SiO_2	52.18	53.77	51.25	53.55	52.48	51.49	52.80	52.72	51.40	52.19	52.19	51.68	51.73	52.16	52.17
TiO_2	0.25	0.33	0.35	0.27	0.31	0.42	0.30	0.25	0.29	0.38	0.21	0.28	0.16	0.38	0.30
Al_2O_3	1.58	1.05	2.62	1.23	1.39	2.24	2.10	1.77	0.38	0.44	0.83	1.36	1.37	0.62	0.39
FeO	19.99	16.99	18.73	18.39	19.58	19.77	17.45	19.99	26.44	24.71	21.58	24.51	24.86	23.58	24.41
MnO	0.35	0.48	0.40	0.62	0.54	0.35	0.34	0.35	0.93	1.00	0.69	0.88	0.75	0.78	0.93
MgO	23.53	25.64	24.61	25.20	24.12	24.03	24.63	23.77	19.21	19.81	22.94	19.96	19.72	20.43	20.18
CaO	1.51	1.82	1.54	1.50	1.61	1.75	1.59	1.53	1.72	1.88	1.77	1.17	1.47	1.86	1.64
Na_2O	0.27	-	0.19	-	0.18	-	0.46	0.28	-	-	0.03	0.18	0.34	-	-
Total	*99.66*	*100.08*	*99.69*	*100.76*	*100.21*	*100.05*	*99.67*	*100.66*	*100.37*	*100.41*	*100.24*	*100.02*	*100.40*	*99.81*	*100.02*
Wo (mol%)	3.02	3.56	3.05	2.93	3.19	3.46	3.20	3.03	3.52	3.82	3.52	2.40	3.01	3.78	3.33
En (mol%)	65.55	69.79	67.92	68.39	66.56	66.13	68.89	65.53	54.55	56.00	63.52	56.95	56.11	57.78	57.06
Fs (mol%)	31.43	26.65	29.03	28.69	30.25	30.40	27.92	31.44	41.94	40.18	32.95	40.65	40.89	38.44	39.60
mg#	0.68	0.73	0.70	0.71	0.69	0.68	0.72	0.68	0.56	0.59	0.65	0.59	0.59	0.61	0.60

(b)	SAV12	SA7	SA35	SAV15	SAV15	SAV15	SAV10	SA15	SA15	SA15	SA15	SA10	SA10	SAV8	SAV8
Unit	LT	LT	LT	P	P	P	LI	LI	LI	LI	LI	LI	LI	LI	LI
	c	c	c	c	r	mph	c	c	r	mph	r	c	r	c	r
SiO_2	50.77	51.01	48.03	48.57	49.57	50.63	49.66	49.66	50.44	51.51	50.44	49.63	50.91	51.51	50.59
TiO_2	0.57	0.52	1.09	0.88	0.85	0.79	0.67	0.67	0.79	0.33	0.79	0.70	0.33	0.33	0.58
Al_2O_3	2.67	1.86	5.12	6.32	5.79	3.43	3.96	3.96	3.88	2.55	3.88	3.13	1.64	2.55	2.63
FeO	10.44	11.42	9.74	7.34	7.88	10.67	11.77	11.77	10.45	10.05	10.45	11.30	12.94	10.05	11.94
MnO	0.16	0.32	0.30	0.15	0.20	0.46	0.39	0.39	0.23	0.00	0.23	0.30	0.45	0.00	0.23
MgO	15.27	16.06	14.08	14.37	14.78	15.11	14.11	14.11	13.98	14.95	13.98	14.27	14.14	14.95	13.55
CaO	19.08	18.36	20.76	20.93	20.53	18.45	18.46	18.46	19.45	19.68	19.45	20.36	19.65	19.68	19.98
Na_2O	0.39	0.24	0.48	0.55	0.44	0.27	0.52	0.52	0.40	0.36	0.40	0.34	0.31	0.36	0.25
Cr_2O_3						0.13									
Total	*99.35*	*99.79*	*99.60*	*99.11*	*100.04*	*99.93*	*99.54*	*99.54*	*99.62*	*99.43*	*99.62*	*100.03*	*100.37*	*99.43*	*99.75*
Wo (mol%)	39.26	37.19	43.08	44.75	43.31	38.31	38.79	38.79	41.17	40.72	41.17	41.58	39.98	40.72	41.33
En (mol%)	43.72	45.27	40.66	42.75	43.39	43.65	41.26	41.26	41.18	43.05	41.18	40.55	40.03	43.05	39.01
Fs (mol%)	17.03	17.54	16.27	12.50	13.31	18.04	19.95	19.95	17.65	16.23	17.65	17.87	20.00	16.23	19.66
mg#	0.72	0.71	0.72	0.78	0.77	0.72	0.68	0.68	0.70	0.73	0.70	0.69	0.66	0.73	0.67

c: phenocryst core ; r: phenocryst rim; mph: microphenocryst; g: groundmass; mg#: MgO/(MgO+FeO) molar, with all iron as Fe^{2+}.

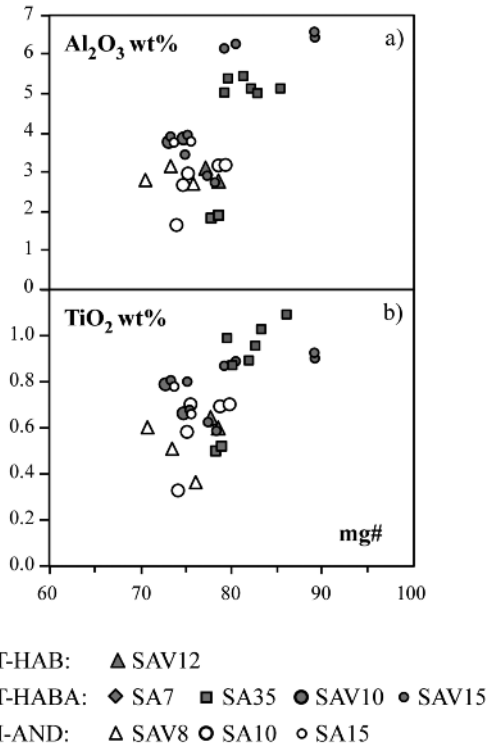

Fig. 3 - Variation diagrams of magnesium number (mg#) *vs* Al_2O_3 (a) and TiO_2 (b) for clinopyroxenes of representative Sant'Antioco samples. Note the difference in Al_2O_3 and TiO_2 contents of clinopyroxenes in lavas with similar evolution degree (i.e., SA7 and SA35 considered for petrogenetic modeling). HAB: high-alumina basalt; HABA: high-alumina basaltic andesite; AND: andesite.

and mafic phases during magma evolution, leading to the observed low-MgO and high-Al_2O_3 compositions (e.g., Pichavant and McDonald, 2007; also see below).

Variation diagrams (Fig. 5) exhibit broad correlations of major oxides with MgO, besides wide scatter (e.g., Al_2O_3 and CaO). As a whole, in spite of distinct field appearance and petrographic features, LI and LT do not define separate compositional trends, whereas both rock groups display correlations consistent with crystallization and removal of the aforementioned phenocryst phases (i.e., plagioclase, pyroxenes, Fe-Ti oxides, olivine). In fact, FeO_t, TiO_2, CaO, and Al_2O_3 are positively correlated with MgO, while SiO_2 and Na_2O are negatively correlated with MgO. The extent of Al_2O_3 and CaO scattering, however, implies at least different mineral phase proportions and/or compositions during fractional crystallization.

Trace elements depict broad correlations with silica, despite considerable scattering. In particular, Rb, Ba, Zr, Y and Nb (TABLE 6, Fig. 6) exhibit an incompatible behaviour, as also evidenced by their mutual positive correlations (not shown). Conversely, V and Sr behave as compatible elements and reflect the progressive removal of Fe-Ti oxides and plagioclase. Cr and Ni display low concentrations (<100 and <60 ppm, respectively; TABLE 6), a typical feature of low-MgO, high-Al_2O_3 arc magmas worldwide, which is related to the prolonged removal of mafic phases during magma differentiation (e.g., Pichavant and Macdonald, 2007 and references therein).

Spider diagrams of trace element concentrations normalized to N-MORB (Sun and Mc Donough, 1989; Fig. 7a), show depletion of HFSE (High Field Strength Elements; with pronounced troughs at Nb and Ti) with respect to LILE (Large Ion Lithophile Elements) and LREE (Light Rare Earth Elements), as it is typical of arc magmas. The whole set of samples shares very similar patterns, with a general enrichment toward the most differentiated rocks and only slight changes in the incompatible/compatible element ratios. The chondrite-normalized REE patterns are also similar for rocks with different degree of evolution (Fig. 7b) and show a slight increase of $(La/Yb)_N$ (from 3.6 to 5.9; subscript N indicates normalized abundances), for near constant $(Sm/Yb)_N$, in the most differentiated rocks. The latter also show a weak Eu trough (Eu/Eu*=0.83-0.88, where Eu* is (Sm+Gd)/2), which instead is lacking in less differentiated rock types (Eu/Eu*=0.93-0.97).

Table 5
Representative electron microprobe analyses of olivine, amphibole and Fe-Ti oxides from the Sant'Antioco study rock-types.

Olivine

Unit	SAV12 LT c	SAV12 LT mph	SA7 LT c	SA35 LT c	SA35 LT r	SA40 LT c	SA40 LT r
SiO_2	35.73	38.70	35.53	37.56	38.58	36.7	38.13
FeO	37.82	32.27	37.86	34.76	36.1	37.7	39.047
MnO	0.64	0.68	0.75	0.52	0.24	0.64	0.50
MgO	26.37	25.94	24.99	25.91	24.18	24.94	22.06
NiO							
CaO	0.64	0.71	0.43	0.47	0.70	0.29	0.41
Total	*100.56*	*97.58*	*99.13*	*98.75*	*99.10*	*99.98*	*99.74*
Fo (mol%)	55.42	58.90	54.06	57.06	54.43	54.12	50.18

	Amphibole			*Fe-Ti oxides*		
Unit	SA34 LI	SA25 F	SA32 LI	SAV8 LI	SAV8 LI	SAV11 LT
SiO_2	47.53	47.71	47.41	-	0.21	-
TiO_2	1.44	1.34	1.45	1.70	45.84	3.12
Al_2O_3	8.68	8.33	8.18	1.43	0.12	1.34
FeO	14.58	13.61	13.79	89.99	50.32	88.39
MnO	0.07	0.12	0.12	0.35	2.13	0.37
MgO	13.75	14.41	14.37	-	0.1	0.33
CaO	10.34	10.54	10.97			
Na_2O	1.36	1.61	1.37			
K_2O	0.21	0.31	0.36			
Total	*97.96*	*97.98*	*98.02*	*93.47*	*98.72*	*93.55*
mg#	0.63	0.65	0.65			

c: phenocryst core ; r: phenocryst rim; mph: microphenocryst; mg# = MgO/(MgO+FeO) molar, with all iron as Fe^{2+}.

Overall, trace element patterns indicate that magmatic evolution was mostly controlled by fractional crystallization, consistent with evidence from major element variations. The wide data point scatter, however, implies that fractional crystallization cannot fully account for the observed chemical variations in the Sant'Antioco volcanics and that an additional process, such as crustal contamination, was likely involved in magma evolution (also see below). This seems to be confirmed by the $^{87}Sr/^{86}Sr$ initial (i.e. at 15 Ma) isotopic ratios for Sant'Antioco whole rocks, which range from 0.70698 to 0.70858±1 (Table 6). Crustal assimilation is also suggested by the positive correlations of the initial Sr isotope ratios with

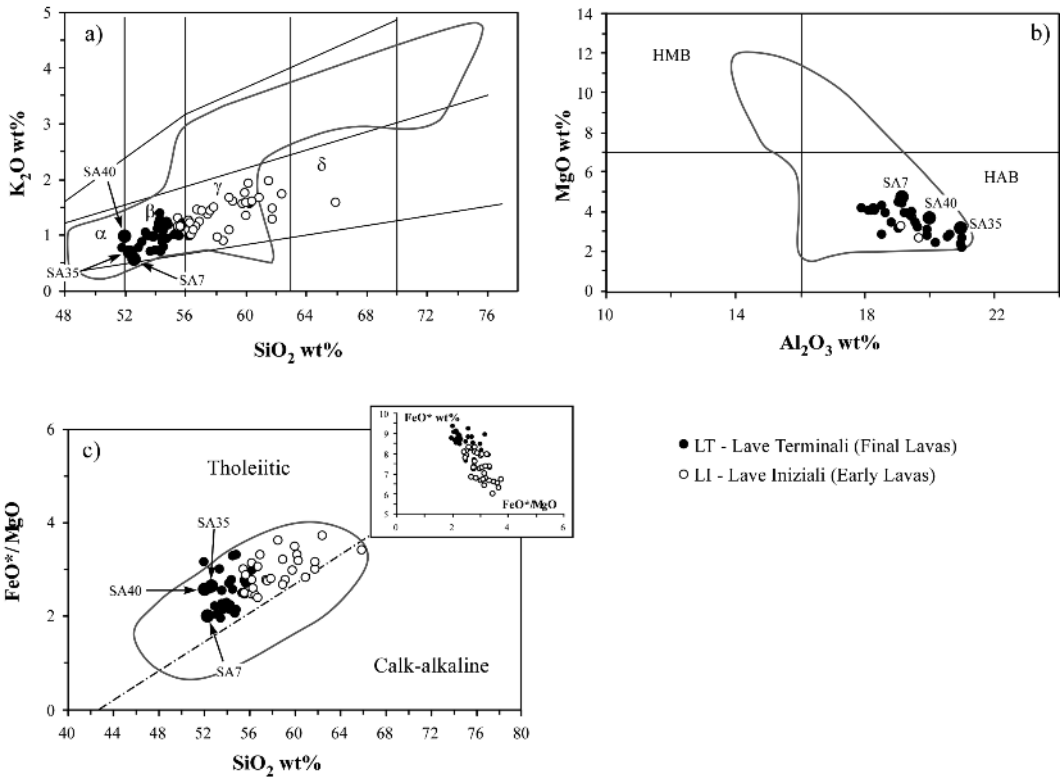

Fig. 4 - Classification diagrams of K_2O *vs* SiO_2 (after Peccerillo and Taylor, 1976) (a), MgO *vs* Al_2O_3 (after Kersting and Arculus, 1994) (b), FeO*/MgO *vs* SiO_2 (after Miyashiro, 1974) (c), for the investigated Sant'Antioco volcanics. Inset in (c) shows the plot of FeO* *vs* FeO*/MgO (* = all iron as FeO). The three samples representative of the least evolved compositions (i.e., SA7, SA35 and SA40) are marked. Solid lines enclose the compositional field of Cenozoic orogenic volcanic rocks of Sardinia (data from literature cited in the text). HMB: high-magnesia basalt; HAB: high-alumina basalt; α: medium-K basalt; β: medium-K basaltic andesite; γ: medium-K andesite; δ: medium-K dacite.

SiO_2 and with some incompatible trace elements sensitive to crustal contamination (i.e., Rb, Ba, Zr), along with the negative correlation with Sr abundance, sensitive to crustal contamination + plagioclase fractionation (Fig. 8).

Estimates of magma temperatures and H_2O concentrations

Geothermometric determinations based on magnetite/Ti-magnetite and ilmenite pairs (Buddington and Lindsley, 1964) are prevented for the Sant'Antioco suite, due to the rare occurrence of coexisting, unexsolved crystals of the two opaque phases in the analyzed samples. Therefore, in order to constrain the crystallization temperatures of magmas, the two-pyroxenes equilibrium geothermometer of Lindsley (1983) was applied. This approach may provide a general indication of temperature even in the lack of coexisting low-Ca pyroxene, by plotting individual augite phenocryst compositions. The projection onto Lindsley's isotherms for P = 500 MPa (preferred to the 1 GPa and 1 atm schemes to constrain the maximum crystallization depth at Sant'Antioco,

Table 6

Representative analyses of major and trace elements from Sant'Antioco study rock-types. $^{87}Sr/^{86}Sr$ isotope ratios of selected samples are also reported.

	EARLY LAVAS (LI)														PISPISIA - M.te ARBUS UNIT (P)						
Sample	SAV7	SA11	SA12	SAV13	SA15	SA10	SA31	SAV18	SA17	SAV5	SAV8	SA34	SA33	SA32	SA27*	SAV15*	SAV14*	SAV19**	SAV17**	SAV16**	SAV20*
[a]Rock-type	HABA	HABA	AND	AND	AND	AND	AND	AND	AND	AND	AND	AND	AND	DAC	HABA	HABA	HABA	HABA	HABA	AND	AND
SiO_2	54.60	54.89	55.19	55.28	55.90	56.82	57.04	57.73	58.02	58.99	59.51	60.33	61.52	65.04	52.68	53.18	53.91	54.51	55.55	56.00	57.22
TiO_2	0.90	1.03	0.96	0.90	0.90	0.93	0.83	0.69	1.00	0.70	0.75	0.71	0.67	0.60	1.07	1.05	0.99	0.96	0.90	0.91	0.70
Al_2O_3	19.43	18.94	19.82	19.09	18.51	18.09	18.48	19.62	17.29	17.86	17.36	17.17	17.00	15.33	18.82	19.17	19.47	18.70	18.96	18.48	19.71
Fe_2O_3	5.00	3.61	4.08	3.36	3.92	2.90	5.07	3.95	4.60	3.17	4.04	4.79	4.63	4.27	3.43	4.42	4.56	3.69	3.82	3.63	3.39
FeO	3.45	4.78	3.19	4.55	4.17	5.36	2.90	2.65	3.71	3.91	3.64	2.24	2.47	2.10	5.53	4.59	4.06	4.99	4.27	4.53	3.36
MnO	0.14	0.16	0.12	0.17	0.16	0.17	0.14	0.12	0.19	0.15	0.15	0.13	0.12	0.13	0.16	0.19	0.17	0.17	0.16	0.16	0.13
MgO	2.61	3.23	2.19	2.12	3.18	2.88	2.68	1.71	2.45	2.16	2.30	2.17	1.79	1.74	4.41	3.76	3.19	3.07	2.58	2.59	1.78
CaO	8.74	8.63	9.02	8.67	8.57	7.66	7.42	8.49	7.31	7.04	6.84	6.63	6.29	5.56	9.37	9.24	9.44	8.63	8.69	8.44	8.57
Na_2O	2.75	2.65	2.62	2.62	2.60	2.74	2.82	2.96	3.01	2.93	2.77	2.57	2.66	2.55	2.30	2.49	2.53	2.30	2.48	2.18	2.78
K_2O	1.30	1.14	1.24	1.45	1.13	1.37	1.49	0.89	1.08	1.73	1.57	1.27	1.70	1.58	1.00	0.72	0.97	1.11	1.07	1.42	0.95
P_2O_5	0.19	0.20	0.18	0.21	0.23	0.25	0.20	0.25	0.28	0.22	0.21	0.22	0.19	0.19	0.16	0.16	0.17	0.20	0.17	0.17	0.26
L.O.I.	0.86	0.69	1.36	1.56	0.71	0.78	0.90	0.91	1.03	1.10	0.83	1.75	0.94	0.89	1.01	0.99	0.51	1.63	1.31	1.43	1.11
	99.97	99.95	99.97	99.98	99.98	99.95	99.97	99.97	99.97	99.96	99.97	99.98	99.98	99.98	99.94	99.96	99.97	99.96	99.96	99.94	99.96
FeO_{total}	*7.95*	*8.03*	*6.86*	*7.57*	*7.70*	*7.96*	*7.47*	*6.21*	*7.85*	*6.76*	*7.28*	*6.55*	*6.64*	*5.95*	*8.62*	*8.57*	*8.16*	*8.31*	*7.71*	*7.80*	*6.41*
mg#	36.9	41.7	36.3	33.3	42.4	39.2	39.0	32.9	35.7	36.3	36.0	37.1	32.5	34.3	47.7	43.9	41.1	39.7	37.4	37.2	33.1
V	212	222	180	191	186	191	188	236	209	153	220	105	136	83	162	180	148	133	142	154	202
Cr	10	12	9	6	12	8	11	10	8	15	6	5	5	6	22	18	14	12	12	10	12
Co	19	20	13	16	12	16	18	18	16	14	14	13	12	20	10	24	20	13	15	19	11
Ni	12	10	7	9	9	8	7	5	5	19	5	6	15	15	13	10	8	7	7	9	5
Rb	38	35	43	42	42	41	48	45	43	60	58	55	59	56	27	29	29	33	47	45	36
Sr	317	299	343	357	313	316	292	329	376	287	289	279	268	250	316	319	301	374	393	379	364
Y	21	28	27	27	26	27	23	24	29	25	27	26	30	33	22	23	25	28	26	23	28
Zr	104	120	141	134	139	133	122	140	130	132	121	145	129	123	98	114	112	125	133	132	207
Nb	5	7	8	7	8	7	7	9	8	8	6	8	7	7	6	5	5	7	6	6	9
Ba	435	326	448	405	412	421	357	530	379	685	448	471	446	503	266	426	330	357	452	400	407
Th	3.9	4.5	4.7	4.5	4.3	4.1	4.1	5.1	4.9	5.8	4.7	5.4	6.5	5.7	2.2	3.1	2.6	3.5	3.9	4.8	5.2
La		18.9				22.0		24.1					26.2	22.1		15.0					
Ce		36.9				44.4		46.7					44.9	43.3		30.4					
Pr		4.47				4.96		5.25					5.53	4.76		3.45					
Nd		21.3				23.7		24.2					24.7	22.1		17.7					
Sm		4.66				5.09		5.24					5.18	4.54		3.83					
Eu		1.45				1.51		1.595					1.48	1.28		1.32					
Gd		4.89				4.96		4.99					5.37	4.34		4.12					
Tb		0.80				0.80		0.79					0.80	0.66		0.65					
Dy		4.76				4.79		4.86					4.93	3.98		4.29					
Ho		0.98				0.97		1.00					1.03	0.8		0.87					
Er		2.91				2.95		3.03					3.11	2.33		2.69					
Tm		0.43				0.43		0.45					0.47	0.34		0.39					
Yb		2.65				2.60		2.98					3.06	2.22		2.39					
Lu		0.43				0.43		0.43					0.48	0.34		0.38					
Hf		3.18				3.51		3.67					3.45	3.21		2.26					
Ta		0.44				0.46		0.55					0.65	0.56		0.49					
U		0.59				0.74		0.81					1.05	1.24		0.61					
$(^{87}Sr/^{86}Sr)_i$	0.70764							0.70807		0.70858						0.70763					

TABLE 6
Continued...

	FINAL LAVAS (LT)										DYKES (F)			
Sample	SAV12	SA40	SA7	SA35	SAV11	SA36	SA3	SA1	SA38	SA9	SA29	SA21	SAV8b	SA25
[a]Rock-type	HAB	HABA	HABA	HABA	HABA	HABA	HABA	HABA	HABA	HABA	HABA	AND	AND	AND
SiO_2	50.86	51.12	51.13	51.68	52.65	53.16	53.23	53.70	54.14	54.38	52.58	55.26	58.93	60.60
TiO_2	1.18	1.07	1.04	1.03	1.03	1.00	1.00	1.00	0.90	1.03	1.12	1.04	0.68	0.85
Al_2O_3	20.23	19.64	18.78	20.68	20.32	19.00	18.36	17.98	20.80	19.66	18.19	18.26	17.99	16.79
Fe_2O_3	4.43	5.09	4.50	4.62	4.42	3.88	3.80	5.77	2.95	3.45	5.37	4.23	3.48	1.99
FeO	5.31	4.48	5.07	3.94	4.07	5.18	4.98	3.30	4.51	4.40	4.07	4.49	3.64	5.13
MnO	0.16	0.18	0.18	0.16	0.16	0.18	0.18	0.18	0.14	0.16	0.18	0.15	0.14	0.17
MgO	2.78	3.56	4.61	3.09	2.68	3.92	3.85	4.00	2.17	3.03	4.19	2.80	2.00	1.57
CaO	10.65	9.90	9.87	10.46	10.11	9.15	9.16	8.79	9.68	8.89	9.45	8.97	7.13	5.78
Na_2O	2.37	2.49	2.07	2.36	2.46	2.45	2.59	2.46	2.65	2.53	2.44	2.33	2.80	3.55
K_2O	0.76	0.96	0.69	0.57	1.03	0.97	1.19	1.17	0.93	1.00	0.69	0.98	1.57	1.94
P_2O_5	0.17	0.18	0.16	0.21	0.21	0.20	0.22	0.23	0.23	0.19	0.22	0.20	0.19	0.28
L.O.I.	1.04	1.31	1.85	1.16	0.81	0.86	1.39	1.05	0.85	1.24	1.46	1.25	1.41	1.30
	99.94	99.97	99.95	99.96	99.95	99.95	99.95	99.63	99.95	99.96	99.96	99.96	99.96	99.95
FeO_{total}	*9.29*	*9.05*	*9.12*	*8.10*	*8.05*	*8.67*	*8.40*	*8.49*	*7.17*	*7.50*	*8.91*	*8.29*	*6.78*	*6.92*
mg#	34.8	41.2	47.4	40.5	37.2	44.6	45.0	45.6	35.0	41.9	45.6	37.6	34.5	28.8
V	279	292	280	252	223	250	265	249	185	206	257	175	117	64
Cr	30	17	100	19	16	16	16	31	26	15	48	16	6	6
Co	21	27	28	17	25	18	23	27	15	19	22	18	15	14
Ni	16	28	41	35	20	34	14	15	15	7	19	7	12	5
Rb	23	27	21	22	26	25	28	33	25	34	23	35	57	67
Sr	338	352	336	398	362	315	355	340	368	302	337	378	280	314
Y	23	24	24	25	23	26	25	25	28	26	24	22	24	35
Zr	89	82	84	80	99	83	102	101	101	126	106	108	121	185
Nb	3	4	4	6	4	4	6	7	6	8	6	7	7	10
Ba	402	322	380	345	397	291	343	301	310	354	378	520	539	482
Th	1.9	2.8	2.4	3.2	2.9	2.6	2.7	2.8	3.1	4.1	2.3	4.4	5.6	6.6
La	13.6	13.4	13.9	13.4		13.2			15.9				22.9	29.9
Ce	27.2	27.8	28.6	28.2		27.4			33.1				41.4	63.4
Pr	3.24	3.29	3.49	3.46		3.35			4.13				5.12	7.12
Nd	16.8	16.6	17.0	17.3		16.7			20.2				22.4	32.3
Sm	3.67	3.87	3.88	3.96		3.83			4.74				4.99	6.69
Eu	1.24	1.24	1.24	1.29		1.24			1.42				1.68	1.78
Gd	3.99	4.08	4.19	4.25		4.20			4.58				4.86	6.42
Tb	0.65	0.69	0.69	0.71		0.70			0.79				0.74	0.98
Dy	4.08	4.11	4.15	4.40		4.34			4.74				4.71	5.94
Ho	0.84	0.83	0.83	0.89		0.89			0.95				1.03	1.19
Er	2.39	2.47	2.55	2.68		2.70			2.86				2.99	3.47
Tm	0.35	0.37	0.35	0.42		0.39			0.42				0.44	0.52
Yb	2.25	2.35	2.28	2.50		2.52			2.74				3.01	3.36
Lu	0.36	0.35	0.35	0.40		0.39			0.42				0.45	0.52
Hf	1.73	2.23	2.27	2.28		2.41			2.72				4.31	4.63
Ta	0.22	0.43	0.29	0.44		0.64			0.59				0.87	0.91
U	0.41	0.52	0.49	0.37		0.54			0.58				0.98	1.13
$(^{87}Sr/^{86}Sr)_i$	0.70716				0.70698								0.70844	

[a] HAB: high-alumina basalt; HABA: high-alumina basaltic andesite; AND: andesite; DAC: dacite.
* lava injection in polygenic breccia;
** lava clasts in polygenic breccia;
mg# = MgO/(MgO+FeO*) molar, with all iron as FeO.

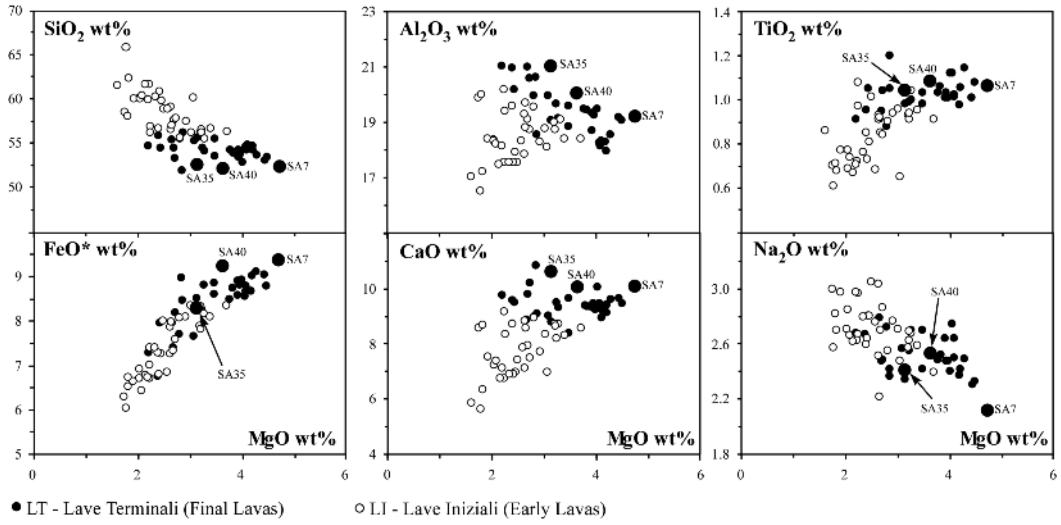

Fig. 5 - Variation diagrams of selected major oxides *vs* MgO for the investigated Sant'Antioco volcanic suite. The three samples representative of the least evolved compositions (i.e., SA7, SA35 and SA40) are marked.

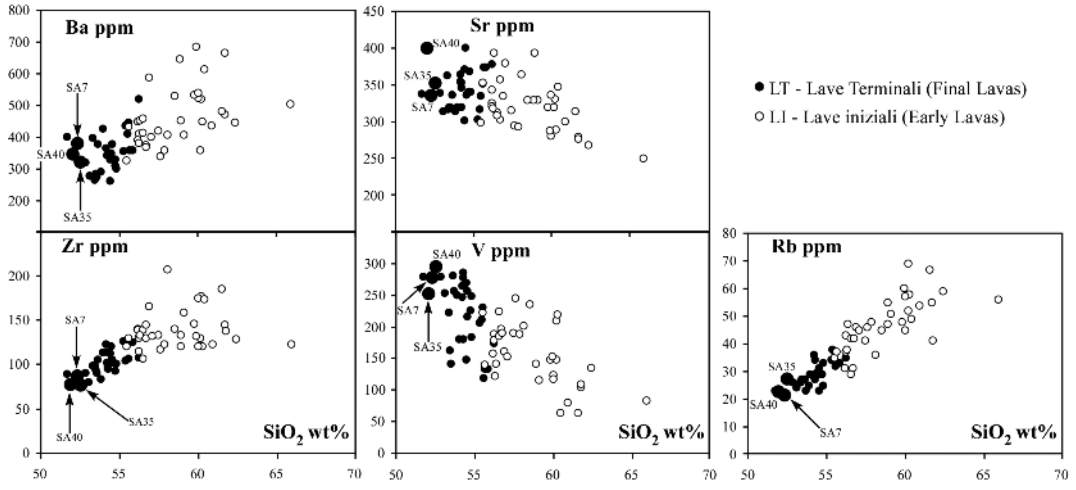

Fig. 6 - Variation diagrams of selected trace elements *vs* SiO_2 for the investigated Sant'Antioco volcanic suite. The three samples representative of the least evolved compositions (i.e., SA7, SA35 and SA40) are marked.

according to the observed phase relationships and MELTS modeling; Ghiorso *et al.*, 1994; see below in this Section) indicates that most temperatures fall in the range of 1000-1150°C. One of the least evolved basaltic-andesites, SA7 (LT), shows the highest equilibration temperature at ~1200°C (Fig. 9).

In addition, crystallization temperatures were

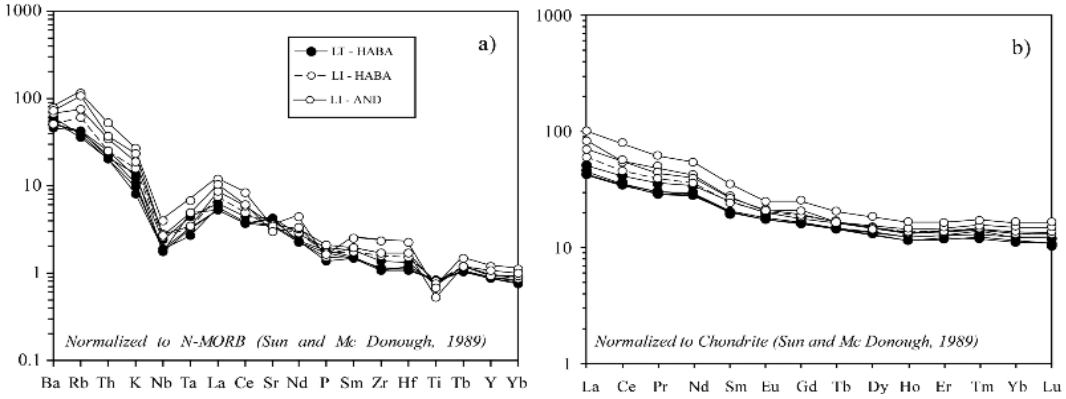

Fig. 7 - Normal MORB-normalized diagram of trace element concentrations (a) and chondrite-normalized REE patterns (b) for representative Sant'Antioco volcanics (HABA: high-alumina basaltic andesite; AND: andesite).

estimated by applying the plagioclase-liquid geothermometer (Putirka, 2008) to the plagioclase cores-whole rock pairs. For these calculations, basaltic andesite and andesite samples characterized by the lowest contents of phenocrysts (either isolated or in glomeri) were selected as the best representative of liquid compositions. The calculated temperature interval of 1100-1165°C broadly matches that obtained through Lindsley's (1983) method.

The amount of dissolved H_2O in the system can be also estimated based on the plagioclase-melt equilibrium equation (Putirka, 2008). Calculations yield H_2O concentrations in the 2.3-3.9 wt% range, where the highest value refers to the highest-Al_2O_3 lava sample (SA35). A similar range of H_2O contents (2.0-4.1 wt%) is derived through the Pichavant and Macdonald (2007) equation (an empirical geohygrometer based on melt compositions for arc basalt melts), using T values obtained from pyroxene geothermometry. Notably, among the least evolved lavas (mg# ≥ 0.4), SA35 records both the highest H_2O content (~4 wt%) and the lowest crystallization temperature (TABLE 7).

The obtained H_2O contents are consistent with the observed plagioclase compositional variations, the An/Ab ratio being sensitive to X_{H_2O} in the melt. From experimental evidence (Sisson and Grove, 1993a, b), the K_D^{Ca-Na} (= X_{Ca}^{Pl} * X_{Na}^{liq} / X_{Na}^{Pl} * X_{Ca}^{liq}) for plagioclase-melt equilibria of high-alumina basalts and basaltic andesites is strongly dependent on H_2O contents and relatively independent on pressure, as it increases from 1.1 (anhydrous conditions) up to 5.5 (H_2O-saturated magmas).

On these grounds, the plagioclase-liquid Ca/Na (molar) diagram provides constraints on the pre-eruptive X_{H_2O} conditions of the studied products (Fig. 10). Concerning high-alumina basaltic andesites, K_D^{Ca-Na} values for microphenocrysts and phenocryst rims *vs* bulk groundmass compositions range from ca. 1.3 to 2.3, most of the data points plotting between the experimental K_D^{Ca-Na} equilibrium lines for anhydrous (K_D^{Ca-Na}=1.1) and 2 wt% H_2O-hydrated melts (K_D^{Ca-Na}=1.7; Fig. 10). Phenocryst cores *vs* whole rock equilibria yield higher K_D^{Ca-Na} values (from ca. 2.6 to 4.5), corresponding to the interval between 2 wt% H_2O (K_D^{Ca-Na}=1.7) and the H_2O-saturated conditions (6 wt% H_2O; K_D^{Ca-Na}=5.52). Phenocryst cores *vs* whole rock data for selected andesites (Fig. 10) reveal lower H_2O concentrations than in basaltic andesites

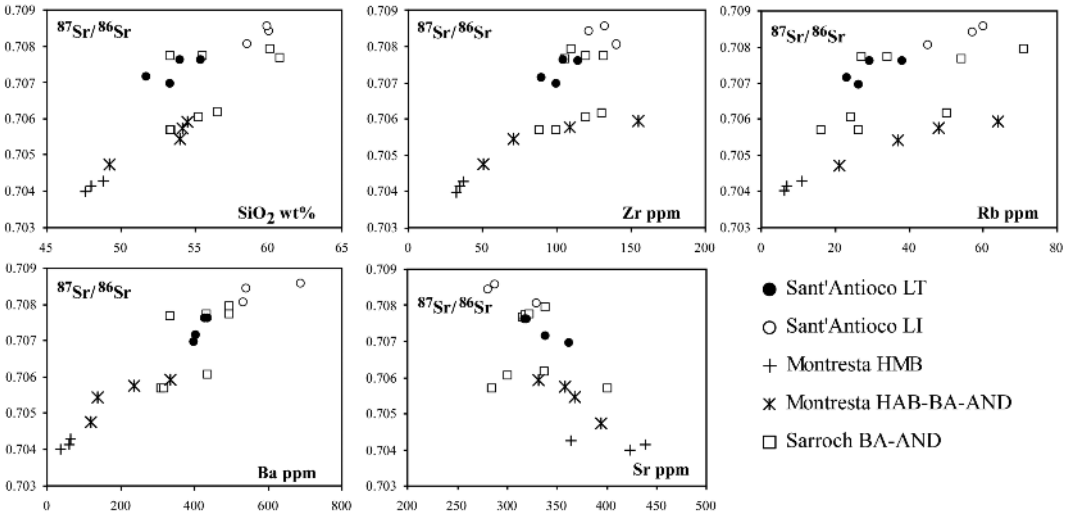

Fig. 8 - Variation diagrams of $^{87}Sr/^{86}Sr$ *vs* SiO_2 and selected trace elements for representative Sant'Antioco mafic volcanics. Data for volcanic rocks from Montresta (HMB: high-MgO basalt, HAB: high-Al_2O_3 basalt, BA: basaltic andesite and AND: andesite) and Sarroch (basaltic andesite and andesite) districts (after Morra *et al.*, 1997 and Conte, 1997) are also reported for comparison.

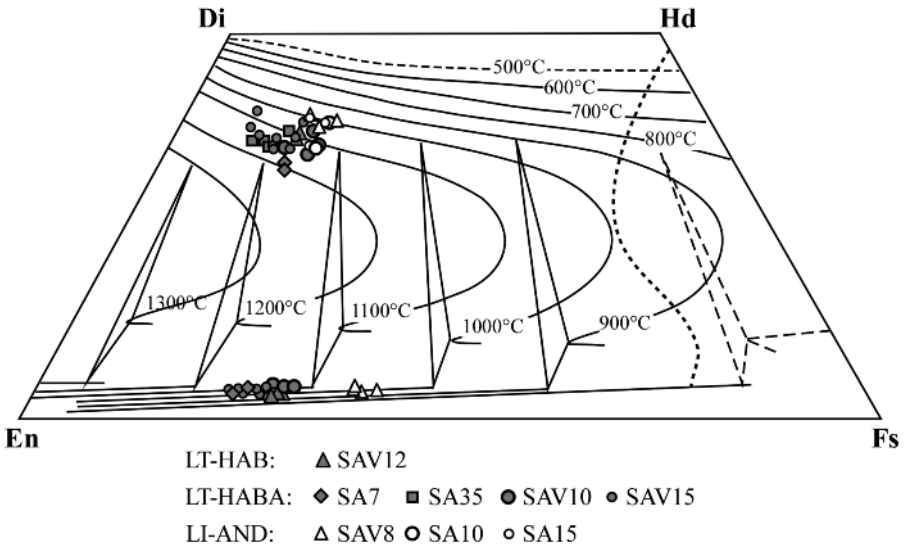

Fig. 9 - Representative analyses of pyroxenes from the Sant'Antioco study suite, projected onto the Di-En-Fs-Hd quadrilater (following Lindsley, 1983). Isotherms are shown for P = 500 MPa, chosen, in preference to 1 GPa or 1 atm, as the most appropriate pressure conditions for magma crystallization in our case study (see text).

TABLE 7

Calculated water contents (H_2O wt%) for selected Sant'Antioco samples, following the methods of Pichavant and McDonald (2007) and Putirka (2008).

Rock samples	Pichavant and Macdonald (2007)	Putirka (2008)
SAV12	3.8	-
SA7	2.6	2.4
SA35	4.1	3.9
SA40	2.5	2.7
SAV11	2.9	2.5
SA15	3.1	-
SAV15b	3.4	2.6
SAV13	3.3	-
SA10	2.4	-
SAV10	3.1	-
SAV5	2.0	2.3
SAV8	3.5	-

(comparable to the values obtained from crystal rims in these latter).

Furthermore, the relationships between the calculated H_2O contents in the melts and plagioclase compositions for some of the least evolved lavas (i.e., SA7, SA40 and SA35) were checked following silicate melt modeling (Ghiorso *et al.*, 1994) for different amounts of dissolved water in the system (1-6 wt%), within the load pressure interval of 100-400 MPa. Model results broadly confirm the above estimated water contents, the latter being the most critical parameter controlling K_D values (rather than mere load pressure). For example, a run at P=100 MPa, T=1110°C and 2 wt% H_2O fits the calculated K_D^{Ca-Na} for phenocryst cores *vs* whole rock for sample SA7, while a run at P=200 MPa, T=1040°C and 5 wt% H_2O yields a K_D^{Ca-Na} matching that obtained for sample SA35. Finally, from pilot experiments performed on the

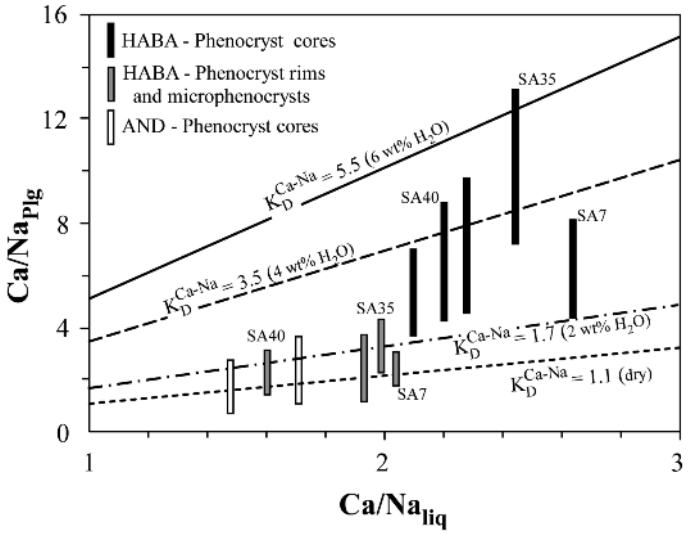

Fig. 10 - Comparison of ⌊Ca⌋/⌊Na⌋ (molar) in plagioclase and coexisting liquid for selected samples from Sant'Antioco volcanics (HABA: high-alumina basaltic andesite; AND: andesite). The three samples representative of the least evolved compositions (i.e., SA7, SA35 and SA40) are marked. Each bar represents the range of values for a single rock-sample. Crystal-liquid equilibria are referred to either phenocryst cores *vs* whole rock compositions or phenocryst rims and microphenocrysts *vs* bulk groundmass compositions. Straight lines represent experimental equilibrium K_D^{Ca-Na} values for anhydrous (K_D^{Ca-Na}=1.1) to H_2O-saturated (K_D^{Ca-Na}=5.5) melts after Sisson and Grove (1993a).

Sant'Antioco least evolved rocks, it has been inferred that SA35 experienced crystallization under significantly higher P_{H_2O} with respect to SA40 and SA7 (Conte *et al.*, 2000).

Petrogenetic inferences

The paucity of primitive magma compositions in subduction-related volcanism worldwide precludes the assessment of the origin of primary magmas, and makes it difficult to distinguish the effects of subcrustal *vs* crustal processes. Similarly, as concerns the rather differentiated lavas from Sant'Antioco, only low-pressure processes involved in their petrogenesis can be addressed here. Indications on source-related processes can be only tentatively drawn by comparison with less-evolved Cenozoic calc-alkaline rocks of Sardinia.

By considering the new set of minero-petrographic and geochemical data, in the light of the huge amount of literature studies on high-alumina arc magmatism, it appears that the wide spectrum of low-MgO (and low Mg#, Ni, Cr), high-alumina rock-types from Sant'Antioco likely reflects extensive fractional crystallization of a parental basaltic liquid, where changes in the fractionating mineral assemblages occurred in response to variable P_{H_2O} conditions (Sisson and Grove, 1993a, b; Pichavant and Macdonald, 2007 and references therein; Ulmer, 2007 and references therein), coupled with crustal interaction at some extent (as suggested by trace element and Sr isotope data; Geochemistry section). On the other hand, the lack of typical disequilibrium textures (i.e., rim resorption, mantling by other phases, reverse or oscillatory zoning) in pyroxene crystals does not support additional low-pressure processes, such as mixing between compositionally different magmas. In this regard, plagioclase dusty textures and zoning patterns are not considered as conclusive evidence of magma mixing and are, instead, thought to be essentially controlled by H_2O conditions (also cfr. Lonis *et al.*, 1997). Even if, in some cases, the observed plagioclase disequilibrium textures and the occurrence of polycrystalline aggregates in LI andesites may point out some crystal recycling in the magma reservoir, we exclude that this process may have significantly affected the chemical evolution of the Sant'Antioco magmas. In this regard, the observed wide scattering in Al_2O_3 and CaO *vs* MgO contents (Fig. 5) would imply unlikely high amounts (some tens vol%) of plagioclase+pyroxenes-bearing glomeri (also cfr. Brotzu *et al.*, 1997a), which do not actually occur in the study volcanics. Moreover, trace element patterns (e.g., the absence of Sr, Eu and Cr positive anomalies) provide no evidence of significant cumulitic processes.

In order to constrain in more detail the petrogenetic processes involved in the studied rock suite, we focus now on the least evolved compositions (i.e., SA7, SA40 and SA35, high-alumina basaltic andesites), which are characterized by different MgO, Al_2O_3, K_2O and FeO contents, in spite of similar SiO_2 contents (around 52 wt%). In Fig. 5, the Al_2O_3-richest sample, SA35, also displays slightly higher CaO and lower FeO contents with respect to the MgO-richest sample, SA7, while sample SA40 shows intermediate contents. Trace element contents are quite similar, except for higher Sr in SA35 and slightly higher Ni and Cr in SA7 (Table 6).

In addition, the three samples are characterized by distinctive phenocryst assemblages, although all plagioclase-dominated (Table 2): the Al_2O_3-richest, phenocryst-poorest, sample SA35 contains the lowest plagioclase amount, and olivine plus rare Cpx as mafic phases; SA40, with intermediate Al_2O_3 content, shows higher abundances of plagioclase and mafic phases, with olivine again prevailing on Cpx; in SA7, the Al_2O_3-poorest and MgO-richest sample, Cpx prevails on olivine, and minor amounts of Opx are also observed.

The three samples also differ in mineral chemistry, being characterized by distinct plagioclase compositions (i.e. An_{75-85}, An_{78-90} and An_{85-93} for SA7, SA40 and SA35, respectively; Fig. 2) and different Al_2O_3 contents in Cpx (from ~2wt% in SA7 up to ~6wt% in SA35), which parallel whole-rock Al_2O_3.

These differences likely indicate that corresponding magmas underwent different pre-eruptive conditions of storage and crystallization, consistent with the above estimated values of temperature, pressure of crystallization and dissolved water content for the three cases. In particular, plagioclase-host liquid equilibria (Fig. 10) provide quantitative information on H_2O contents in the three magmas at different evolutionary stages (the liquid compositions being roughly represented by either the whole-rock or groundmass bulk compositions with ongoing magma crystallization).

Water content data broadly fit the above-reported mineralogical features of samples. In fact, it has been proven that high dissolved H_2O concentrations in high-alumina melts, not only favour the early formation of spinel and the crystallization of An-richer plagioclase, but also reduce the total proportion of plagioclase in the crystallizing assemblage, expand the stability field of olivine at the expense of other mafic phases such as Cpx and Opx, and decrease the En-Fs contents of Cpx in favour of CaTs (Kushiro, 1969; Sisson and Grove, 1993a; Pichavant and Macdonald, 2007).

These considerations lead us to conclude that changes in phenocryst proportions and compositions (and consequent changes in bulk rock chemistry) in the least evolved basaltic andesites were determined by different H_2O concentrations in the melts and by the physical conditions controlling water exsolution from the system during magma ascent. In summary: the Al_2O_3-richest, MgO-poorest sample (SA35) displays, consistent with the highest X_{H_2O} (up to ca. 6 wt%, Fig.10), the lowest modal amount of plagioclase, accompanied by the Ca-richest composition, a paucity of Cpx, with the Ca-Ts-richest augite composition, and the presence of olivine. Conversely, the MgO-richest, Al_2O_3-poorest composition of SA7, may reflect a crystallization path under H_2O-poorer conditions (up to ca. 3 wt%), which favoured the crystallization of higher amounts of Ca-poorer plagioclase and Al_2O_3-poorer Cpx, as well as the occurrence of Opx at the expense of olivine. SA40, which shows intermediate Al_2O_3 and MgO contents, consistently accounts for intermediate H_2O concentration in the magma (up to ca. 4 wt%). In this picture, the Ab-richer plagioclase rims and microphenocrysts in the three samples may testify late H_2O exsolution.

Moreover, modes of water retention/exsolution in the system influence the amphibole stability field. Notably, amphibole only occurs in two LI samples, which records prolonged H_2O retention in the corresponding magmas; late-stage processes of decreasing pressure and H_2O exsolution, causing amphibole break-down, are testified by the presence of opacitic rims.

The effect of X_{H_2O} on phase equilibria thus may represent the key factor in determining the observed geochemical differences among the least evolved Sant'Antioco rock-types, as a result of different evolution paths from a possible common parental melt.

Identification of the parental magma

As it is typical of arc-related magmatism worldwide (e.g., Nye and Reid, 1986; Brophy, 1989; Eggins, 1993; Sisson and Grove, 1993b; Rohrbach *et al.*, 2005; Pichavant *et al.*, 2002; Pichavant and Macdonald, 2007), in Cenozoic orogenic magmatism of Sardinia, high-magnesia basalts (HMBs, MgO >8 wt%), possibly representative of mantle-derived magmas, are relatively uncommon and limited to a few areas (Mattioli *et al.*, 2000 and references therein). In

particular, HMBs from the Montresta district, NW Sardinia (18.5 Ma, Montigny *et al.*, 1981; Morra *et al.*, 1997; Fig. 1) could match in composition the possible precursor for Sant'Antioco LT basaltic andesites. In fact, the high-Al_2O_3 basaltic andesites derived from Montresta HMBs through fractional crystallization±assimilation processes (Morra *et al.*, 1997) show major and trace element compositions that closely resemble those from Sant'Antioco (Fig. 11, 12), except for significantly lower Ba contents (e.g., 140-250 *vs* 300-400 ppm, for Montresta and Sant'Antioco HABA, respectively; Fig. 8).

If a typical Montresta HMB (e.g., sample KB13, MgO = 9.08 wt%, Morra *et al.*, 1997) is chosen as representative of the Sant'Antioco parental magma composition, major element mass balance calculations (following Stormer and Nicholls, 1978) broadly indicate that samples SA7, SA40 and SA35 may be consistently derived by fractional crystallization under different P_{H_2O} conditions (Table 8). Notably, the results yield similar fractions of residual liquid for the three cases (~45-50 wt%), but different proportions of the main crystal phases (especially plagioclase *vs* mafic phases), i.e.: Plg/(Ol+Cpx)=0.52, 0.36 and 0.24 for SA7, SA40 and SA35, respectively.

The similar fractions of residual liquid may account for the similar contents in the majority of incompatible trace elements in the three cases, whereas the observed differences in the Sr contents can be explained by the different amounts of plagioclase fractionation (Fig. 6; 7a, b).

It is also worth noting that relatively high X_{H_2O} conditions *ab initio*, which determine the fractionation of high proportions of mafic phases (with high MgO/FeO* ratios), with respect to plagioclase, may even result in the observed ambiguous tholeiitic character of the Sant'Antioco mafic volcanics (Fig. 4). In our interpretation, this inference could also apply to the "tholeiitic" lavas in the Montresta district (Morra *et al.*, 1997).

Magma evolution

From the whole compositional spectrum of the studied Sant'Antioco volcanics it appears that the differences existing in the least evolved compositions also reflect in the differentiation products (Fig. 5, 11). Major-element mass-balance calculations (Table 9) show that the latter can be derived through prolonged fractional crystallization of Plg + Cpx + Fe-Ti oxides ± Ol ± Opx mineral assemblages. In more detail, if SA35 and SA7 lava-types, which display the most significant differences in terms of oxide concentrations and H_2O contents, are considered as starting melts, the results of calculations evidence that olivine continues to play a role in the early stages of the H_2O-rich differentiation trend starting from SA35 (Fig. 11), while Opx may replace olivine in the fractionating crystal assemblage along the H_2O-poor differentiation trend starting from SA7 (Fig. 11, Table 9). These results confirm, also in agreement with experimental evidence (Pichavant and Macdonald, 2007 and references therein), that in mafic to intermediate calc-alkaline magmas Opx is stable only under low H_2O concentrations, while in more hydrous conditions Opx crystallization is delayed and takes place extensively only in SiO_2-richer magmas at lower temperatures. Indeed, in the Sant'Antioco volcanics, like in other typical arc-rock suites (e.g., Macdonald *et al.*, 2000), Opx is always present in the most differentiated rocks (SiO_2 >55 wt%; Table 9). In more hydrous melts, Opx crystallization is joined by amphibole during the late differentiation stages.

However, simple fractional crystallization cannot fully explain the whole compositional spectrum of the study rock suite. In this regard, the above reported $^{87}Sr/^{86}Sr$ data (0.70698 to 0.70858±1; Table 2; Fig. 8) are in the 0.70398-0.71130 range pertaining to the Cenozoic

TABLE 8

Modeled fractionation steps (following Stormer and Nicholls, 1978) for the least evolved basaltic andesites from Sant'Antioco, starting from a typical high-magnesia basalt of Montresta, inferred as possible parental magma.

	From HMB-KB13 (Montresta district) to HABA's (Sant'Antioco district)						
		from KB13 to SA35		from KB13 to SA40		from KB13 to SA7	
	KB13*	SA35	*residuals*	SA40	*residuals*	SA7	*residuals*
SiO_2	48.88	52.54	0.02	52.06	0.00	52.34	0.04
TiO_2	0.75	1.04	0.00	1.09	0.01	1.07	0.01
Al_2O_3	15.55	21.02	0.00	20.00	0.00	19.22	0.02
FeO*	10.16	8.27	0.02	9.27	0.04	9.38	0.05
MnO	0.12	0.16	0.00	0.18	0.02	0.18	0.01
MgO	9.08	3.14	0.00	3.63	0.02	4.72	0.00
CaO	12.90	10.63	0.01	10.08	0.01	10.11	0.01
Na_2O	1.81	2.40	0.14	2.53	0.05	2.12	0.26
K_2O	0.52	0.58	0.05	0.98	0.00	0.70	0.04
P_2O_5	0.23	0.21	0.02	0.18	0.02	0.16	0.03
	100.00	100.00		100.00		100.00	
$\sum r^2$			0.25		0.16		0.48
	Removed crystals (wt%)						
Ol		11.89		10.46		8.17	
Cpx		28.41		28.18		27.51	
Plg		9.57		13.74		18.66	
Fe-Ti oxides		0.10				0.75	
wt% of residual liquid		50.03		47.62		44.91	
Cpx/Ol		2.39		2.70		3.37	
Cpx+Ol		40.30		38.63		35.68	
Plg/(Cpx+Ol)		0.24		0.36		0.52	

$\sum r^2$: Sum of squared residuals; other abbreviations as in TABLE 2; * compositions of whole rock and mineral phases from Morra *et al.* (1997). For each step of mass balance, the compositions of removed crystals are taken from phenocryst phases (usually rim compositions) from the corresponding parent rocks (see TABLE 3, 4, 5).

Table 9

Modeled fractionation steps (following Stormer and Nicholls, 1978) for the basaltic andesites and andesites of the Sant'Antioco suite, starting from SA7 and SA35 compositions, as discussed in the text.

From SA7 to SA15b to SA32b

	SA7	SA15b	residuals	SA32b	residuals
SiO_2	52.34	56.68	0.00	60.88	0.01
TiO_2	1.07	0.95	0.12	0.73	0.10
Al_2O_3	19.22	18.43	0.00	17.57	0.00
FeO*	9.38	8.11	0.00	6.81	0.01
MnO	0.18	0.15	0.00	0.13	0.00
MgO	4.72	3.38	0.00	2.40	0.00
CaO	10.11	8.32	0.00	6.90	0.00
Na_2O	2.12	2.59	0.01	2.64	0.03
K_2O	0.70	1.16	0.00	1.67	0.01
P_2O_5	0.16	0.22	0.00	0.25	0.00
	100.00	100.00		100.00	
$\sum r^2$		0.13		0.16	

Removed crystals (wt%)

Ol		
Cpx	6.84	3.38
Opx	6.28	4.21
Plg	23.7	16.23
Fe-Ti oxides	2.86	2.19
wt% of residual liquid	39.68	73.99

From SA35 to SA16 to SAV18

	SA35	SA16	residuals	SAV18	residuals
SiO_2	52.54	54.50	0.01	58.49	0.04
TiO_2	1.04	1.05	0.02	0.70	0.17
Al_2O_3	21.02	20.20	0.00	19.88	0.02
FeO*	8.27	7.96	0.00	6.32	0.04
MnO	0.16	0.14	0.00	0.12	0.00
MgO	3.14	2.43	0.00	1.74	0.00
CaO	10.63	9.53	0.00	8.60	0.02
Na_2O	2.40	2.81	0.00	3.00	0.00
K_2O	0.58	1.10	0.10	0.90	0.17
P_2O_5	0.21	0.26	0.00	0.25	0.01
Sum	100.00	100.00		100.00	
$\sum r^2$			0.15		0.48

Removed crystals (wt%)

Ol	2.97	
Cpx	2.58	3.71
Opx		2.93
Plg	12.46	17.94
Ox	0.35	2.88
wt% of residual liquid	81.64	72.54

$\sum r^2$: Sum of squared residuals; other abbreviations as in Table 2. Additional explanations as in Table 8.

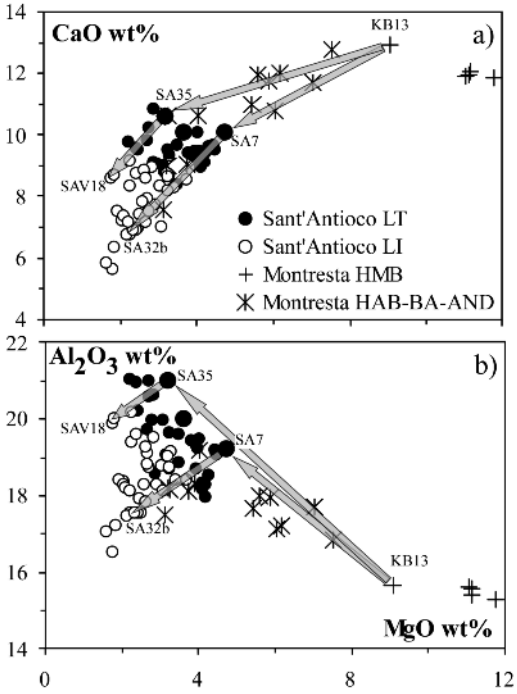

Fig. 11 - Plot of CaO (a) and Al_2O_3 (b) *vs* MgO contents for the investigated Sant'Antioco volcanics, compared with Montresta (data after Morra *et al.*, 1997; rock abbreviations as in Fig. 8). Arrows represent possible differentiation paths, as considered in mass balance calculations (TABLE 8, 9). Samples marked are discussed in the text.

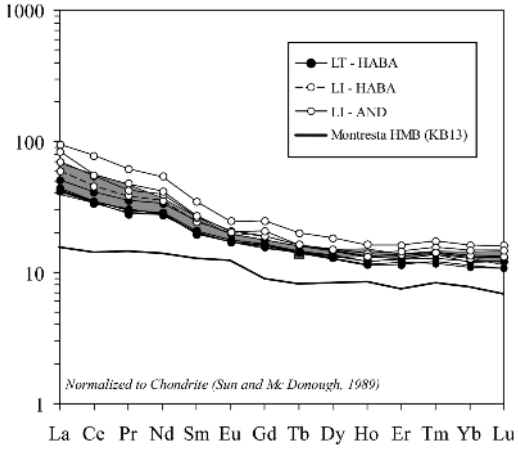

Fig. 12 - Representative REE patterns for high-Al_2O_3 basaltic andesites (HABA) and andesites (AND) from Sant'Antioco and Montresta (shaded field; data after Morra *et al.,* 1997). The pattern for the Montresta high-MgO basaltic sample (HMB, KB13), considered as parental magma in petrogenetic modeling, is also reported (data after Morra *et al.*, 1997).

orogenic rocks of Sardinia (Dupuy *et al.*, 1974, 1979; Coulon, 1977; Brotzu *et al.*, 1997a, b; Conte, 1997; Morra *et al.*, 1997; Downes *et al.*, 2001), for which different degrees of crustal contamination, coupled with variable enrichment of mantle source by subducted sediments, has been proposed. At Sant'Antioco, the observed range of Sr isotope data, the positive correlation of $^{87}Sr/^{86}Sr$ *vs* elements with crustal affinity (e.g., Si, Rb, Ba; Fig. 8), as well as the wide scattering of trace elements (Fig. 6), strongly suggest contamination by crustal wall rocks. In particular, the Sant'Antioco $^{87}Sr/^{86}Sr$ values are significantly higher with respect to the chemically analogous products of Montresta, whereas they overlap the higher values from the nearby Sarroch volcanic district (Fig. 8). In the latter, crustal assimilation has been revealed and quantified in about 4-14 wt% (Conte, 1997), where the assimilated material considered, i.e. an average composition of the granitoid batolith of Sardinia (from Del Moro *et al.*, 1975; Secchi *et al.*, 1991), would account for the observed trace element enrichment (e.g., Ba, Rb and Zr) and depletion (e.g., Sr) trends. Besides the oversimplified assumption concerning the crustal material involved, considering the similar $^{87}Sr/^{86}Sr$ ratios and trace elements behaviour observed for Sant'Antioco and Sarroch volcanics, we infer that crustal contamination affected magma evolution at Sant'Antioco at analogous, or even slightly higher, extent.

CONCLUDING REMARKS

The present work integrates the petrological knowledge on the Cenozoic orogenic magmatism of western Sardinia, with focus on mafic to intermediate rock-types. New data on

Sant'Antioco relatively mafic volcanics, mostly represented by basaltic andesites and andesites, reveal a remarkably wide compositional spectrum in terms of Al_2O_3, MgO and CaO contents, as related to the characterizing mineral assemblages. The observed variability in whole rock and mineral chemistry likely correlates to different liquid lines of descent, controlled by the P_{H_2O} histories of magma systems, starting from a common parental magma composition. The latter has been identified as a high-MgO basalt similar in composition to the broadly coeval Montresta primitive lavas. Different from the Montresta district, the Sant'Antioco area is characterized by the lack of primitive terms, possibly indicating different local tectonic regime favouring magma ponding and differentiation at upper crustal levels.

The overall geochemical features of the Sant'Antioco study rock-types evidence a clear calc-alkaline signature, despite relatively high values of FeO*/MgO that could mimic a misleading tholeiitic affinity. Starting from the composition of a Montresta HMB, considered as a suitable primitive (possibly near-primary) magma, two end-member differentiation trends are recognized, which lead respectively to the MgO-richest/Al_2O_3-poorest and MgO-poorest/Al_2O_3-richest basaltic andesites, representing the least evolved rock-types at Sant'Antioco. These trends can be respectively explained by higher proportions of plagioclase *vs* olivine+Cpx in the fractionating assemblage under H_2O-poorer conditions and *vice versa* in H_2O-richer conditions. Basically, the X_{H_2O} imprint is recorded up to the most evolved compositions, being also the main controlling factor of incoming Opx crystallization.

Finally, Sr isotope data and the trends of trace elements of "crustal affinity" with increasing degree of magma evolution, indicate that different degrees of crustal contamination also played a significant role in the petrogenesis of Sant'Antioco volcanics, consistent with magma slow ascent and ponding within a tick crust in multiple reservoirs and/or feeder conduits that behaved independently.

Acknowledgements

Sincere thanks to F. Secchi and an anonymous referee for their meaningful and constructive review.

Appendix A: Analytical methods

Whole-rock samples were analyzed for major and selected trace elements (V, Cr, Co, Ni, Rb, Sr, Y, Zr, Nb, Ba, Th) by a Philips PW1480-XRF spectrometer at IGG-CNR, Rome, using fused dishes (major element) and pressed powder pellets (trace elements). Philips X40 software was used for data reduction. Analytical precision is generally better than 3% and 5% , for major and trace elements, respectively.

LOI was determined after the samples had been kept at 1050°C for 2 h; resulting losses were corrected for FeO oxidation and FeO was measured by titration with KMnO after acid digestion.

REE, Ta, Hf and U were determined by ICP-MS at the Activation Laboratories, Ancaster, Canada.

Sr isotope ratios were measured, after sample dissolution and ion exchange separation procedures, on a VG354 double collector mass spectrometer at the University Federico II, Naples. Repeated analyses of NBS-987 international reference standard gave an average value of 0.71027±0.00001 (2σ).

Mineral analyses were carried out using a Cameca SX50 electron microprobe with an accelerating voltage of 15 keV and 15 nA beam current at C.N.R.-IGAG, Rome, using the ZAF correction procedure.

REFERENCES

Aramaki S. and Katsura T. (1973) - *Petrology and*

liquidus temperature of the magma of the 1970 eruption of Akita-Komagatake Vocano, northeastern Japan. J. Assoc. Min. Petrol. Econ. Geol., **68**, 101-124.

Araña V., Barberi F. and Santacroce R. (1974) - *Some data on the comendite type area of S. Pietro and S. Antioco islands, Sardinia*. Bull. Volcanol., **38**, 1-12.

Assorgia A., Fadda A., Gimeno Torrente D., Morra V., Ottelli L. and Secchi F. (1990) - *Le successioni ignimbritiche terziarie del Sulcis (Sardegna sud-occidentale)*. Mem. Soc.. Geol. It., **45**, 951-963.

Beccaluva L., Coltorti M., Galassi B., Macciotta G. and Siena F. (1994) - *The Cainozoic calcalkaline magmatism of Westen Mediterranean and its geodynamic significance*. Boll. Geofis. Teor. Appl., **36**, 293-308.

Brophy J.G. (1989) - *Can high-alumina arc basalt be derived from low-alumina arc basalt? Evidence from Kanaga island, Aleutian arc, Alaska*. Geology, **17**, 333-336.

Brotzu P., Callegari E., Morra V. and Ruffini R. (1997a) - *The orogenic basalt-andesite suites from the Tertiary volcanic complex of Narcao, SW-Sardinia (Italy): petrology, geochemistry and Sr-isotope characteristics*. Per. Mineral., **66**, 101-150.

Brotzu P., Lonis R., Melluso L., Morbidelli L., Traversa G. and Franciosi L. (1997b) - *Petrology and evolution of calcakaline magmas from the Arcuentu volcanic complex (SW Sardinia, Italy)*. Per. Mineral., **66**, 151-184.

Buddington A.F. and Lindsley D.H. (1964) - *Iron-Titanium minerals and synthetic equivalents*. J. Petrol., **5**, 310-357.

Cherchi A. and Montadert L. (1982) - *The Oligo-Miocene rift of Sardinia and early history of the western Mediterranean basin*. Nature, **298**, 736-739.

Conte A.M. (1997) - *Petrology and geochemistry of Tertiary calcalkaline magmatic rocks from the Sarroch district (Sardinia, Italy)*. Per. Mineral., **66**, 63-100.

Conte A.M., Argenti E., Palladino D.M. and Trigila R. (2000) - *Magma evolution of S. Antioco volcanics (Sardinia, Italy) as evidenced from laboratory experiments and thermochemical calculations*. EMPG VIII, J. of Conference Abstracts, 5,1, p.25.

Coulon C. (1977) - *Le volcanism calco-alcalin cénozoïque de la Sardaigne (Italie). Petrographie, géochimie et genese des laves andesitiques et des ignimbrites - signification géodinamique.* Ph.D. Thesis, Univ. Aix-Marseille III, pp. 288.

Del Moro A., Di Simplicio P., Ghezzo C., Guasparri G., Rita F. and Sabatini G. (1975) - *Radiometric data and Intrusive Sequence in the Sardinian Batholith*. N. Jb. Miner. Abh., **126**, 28-44.

Doglioni C. (1991) - *A proposal of kinematic modeling for W-dipping subductions - possible application to the Tyrrhenian-Apennines system*. Terra Nova, **3**, 423-434.

Doglioni C., Gueguen E., Harabaglia P. and Mongelli F. (1999) - *On the origin of W-directed subduction zones and applications to the western Mediterranean*. Geol. Soc. Lond. Spec. Publ., **156**, 541-561.

Dostal J., Coulon C. and Dupuy C. (1982) - *Cainozoic andesite rocks of Sardinia (Italy)*. In: Thorpe R.S. (Ed.), Andesites: Orogenic Andesites and Related Rocks. Wiley, Chichester, pp. 353-370.

Downes H., Thirlwall M.F. and Trayhorn S.C. (2001) - *Miocene subduction-related magmatism in southern Sardinia: Sr-Nd and oxygen isotopic evidence for mantle source enrichment.* J. Volcanol. Geotherm. Res., **106**, 1-21.

Dupuy C., Mc Nutt R.H. and Coulon C. (1974) - *Déterminasion de $^{87}Sr/^{86}Sr$ dans les andésites cénozoïques et les laves associées de Sardaigne Nord-Occidentale (Italie)*. Geochim. Cosmochim. Acta, **38**, 1287-1296.

Dupuy C., Dostal J. and Coulon C. (1979) - *Geochemistry and origin of andesitic rocks from northwestern Sardinia.* J. Volcanol. Geotherm. Res., **6**, 375-389.

Egger A., Demartin M., Ansorge J., Banda E. and Maistrello M. (1988) - *The gross structure of the crust under Corsica and Sardinia*. Tectonophysics, **150**, 363-389.

Eggins S.M. (1993) - *Origin and differentiation of picritic arc magmas, Ambae (Aoba), Vanuatu.* Contrib. Mineral. Petrol., **114**, 79-100.

Franciosi L., Lustrino M., Melluso L., Morra V. and D'Antonio M. (2003) - *Geochemical characteristics and mantle sources of the Oligo-Miocene primitive basalts from Sardinia:The role of subduction components*. Ofioliti, **28**, 105-114.

Ghiorso M.S., Hirschmann M.M. and Sack R.O. (1994) - *MELTS: software for thermodynamic modeling of magmatic systems.* EOS, **75**, 574-576.

Kersting A.B. and Arculus R.J. (1994) - *Klyuchevskoy Volcano, Kamchatka, Russia: The role of high-flux recharged, tapped and fractionated magma chamber(s) in the genesis of High-Al_2O_3 from High-MgO basalt*. J. Petrol., **35**, 1-41.

Kuno H. (1959) - *Origin of Cenozoic petrographic provinces in Japan and surrounding areas*. Bull. Volcanol., **20**, 37-76.

Kushiro I. (1969) - *The system forsterite-diopside-silica with and without water at high pressure*. Am. J. Sci., **267A**, 269-294.

Leake B.E., Woolley A.R., Birch W.D., Burke E.A.J., Ferraris G., Grice J.D., Hawthorne F.C., Kisch H.J., Krivovichev V.G., Schumacher J.C., Stephenson N.C.N. and Whittaker E.J.W. (2004) - *Nomenclature of amphiboles: additions and revisions to the International Mineralogical Association's amphibole nomenclature*. Eur. J. Mineral., **16**, 190-195.

Le Bas M.J., Le Maitre R.W., Streckeisen A. and Zanettin R. (1986) - *A chemical classification of volcanic rocks based on the total alkali-silica diagram*. J. Petrol., **27**, 745-750.

Lecca L., Lonis R., Luxoro S., Melis E., Secchi F. and Brotzu P. (1997) - *Oligo-Miocene volcanic sequences and rifting stages in Sardinia: a review*. Per. Mineral., **66**, 7-61.

Lindsley D.H. (1983) - *Piroxene thermometry*. Am. Mineral., **68**, 477-493.

Lonis R., Morra V., Lustrino M., Melluso L. and Secchi F. (1997) - *Plagioclase Textures, Mineralogy and Petrology of Tertiary Orogenic Volcanic Rocks from Sindia (Central Sardinia)*. Per. Mineral., **66**, 7-61.

Lustrino M., Melluso L. and Morra V. (2002) - *The transition from alkaline to tholeiitic magmas: A case study from the Orosei-Dorgali Pliocene volcanic district (NE Sardinia, Italy)*. Lithos, **63**, 83-113.

Lustrino M., Morra V., Melluso L., Brotzu P., D'Amelio F., Fedele L., Franciosi L., Lonis R. and Petteruti Liebercknecht A.M. (2004) - *The Cenozoic igneous activity of Sardinia*. Per. Mineral., **73**, 105- 134.

Lustrino M., Morra V., Fedele L. and Serracino M. (2007) - *The transition between "orogenic" and "anorogenic" magmatism in the western Mediterranean area: the Middle Miocene volcanic rocks of Isola del Toro (SW Sardinia, Italy)*. Terra Nova, **19**, 148-159.

Lustrino M., Morra V., Fedele L. and Franciosi L. (2009) - *Beginning of the Apennine subduction system in central western Mediterranean: Constraints from Cenozoic "orogenic" magmatic activity of Sardinia, Italy*. Tectonics, **28**, TC5016, doi:10.1029/2008TC002419.

Luxoro S. (1987) - *Il vulcanesimo "andesitico" dell'Isola di Sant'Antioco, rilevamento geologico*. B.A. Thesis, Università degli Studi di Cagliari, pp. 137.

Maccioni L., Marchi M. and Assorgia A. (1990) - *Carta Geopetrografica dell'Isola di Sant'Antioco, Sardegna*. Dipartimento di Scienze della Terra, Università di Cagliari.

Macdonald R., Hawkesworth C.J. and Heath E. (2000) - *The Lesser Antilles volcanic chain: a study in arc magmatism*. Earth Sci. Rev., **49**, 1-76.

Mattioli M., Guerrera F., Tramontana M., Raffaelli G. and D'Atri M. (2000) - *High-Mg Tertiary basalts in Southern Sardinia (Italy)*. Earth Planet. Sci. Lett., **179**, 1-7.

Miyashiro A. (1974) - *Volcanic rock series in island arcs and active continental margins*. Am. J. Sci., **274**, 321-355.

Montigny R., Edel J.B. and Thuizat R. (1981) - *Oligo-Miocene rotation of Sardinia: K-Ar ages and paleomagnetic data of Tertiary volcanism*. Earth Planet. Sci. Lett., **54**, 261-271.

Morra V., Secchi F.A. and Assorgia A. (1994) - *Petrogenetic significance of peralkaline rocks from Cenozoic calcalkaline volcanism from SW Sardinia, Italy*. Chem. Geol., **118**, 109 -142.

Morra V., Secchi F.A.G., Melluso L. and Franciosi L. (1997) - *High-Mg subduction-related Tertiary basalts in Sardinia (Italy)*. Lithos, **40**, 69-91.

Nye C.J. and Reid M.R. (1986) - *Geochemistry of primary and least fractionated lavas from Okmok volcano, central Aleutians: implications for arc magma genesis*. J. Geophys. Res., **91**, 10271-10287.

Peccerillo A. and Taylor S.R. (1976) - *Geochemistry of Eocene calc-alkaline volcanic rocks from the Kastamonu area, northern Turkey*. Contrib. Mineral. Petrol., **58**, 63-81.

Pichavant M., Mysen B.O. and Macdonald R. (2002) - *Source and H_2O content of high-MgO magmas in island arc settings: an experimental study of a primitive calc-alkaline basalt from St. Vincent, Lesser Antilles arc*. Geochim. Cosmochim. Acta, **66**, 2193-2209.

Pichavant M. and Macdonald R. (2007) - *Crystallization of primitive basaltic magmas at crustal pressures and genesis of the calc-alkaline igneous suite: experimental evidence from St Vincent, Lesser Antilles arc*. Contrib. Mineral. Petrol., **154**, 535-558.

Pioli L. and Rosi M. (2005) - *Rheomorphic structures in a high-grade ignimbrite: The Nuraxi tuff, Sulcis volcanic district (SW Sardinia, Italy)*. J. Volcanol. Geotherm. Res., **142**, 11-28.

Pioli L., Lanza R., Ort M. and Rosi M. (2008) - *Magnetic fabric, welding texture and strain fabric in the Nuraxi Tuff, Sardinia, Italy*. Bull. Volcanol., **70**, 1123-1137.

Putirka K.D. (2008) - *Thermometers and Barometers for volcanic Systems*. In: Putirka K.D. and Tepley F.J. III (Eds.), Minerals, inclusions and volcanic processes, Reviews in Mineralogy & Geochemistry, **69**, The Mineralogical Society of America, Washington D.C., pp. 61-120.

Rohrbach A., Schuth S., Ballhaus C., Münker C., Matveev S. and Qopoto C. (2005) - *Petrological constraints on the origin of arc picrites, New Georgia group, Solomon islands*. Contrib. Mineral. Petrol., **149**, 685-698.

Sartori, R., Torelli L., Zitellini N., Carrara G., Magaldi M. and Mussoni P. (2004) - *Crustal features along a W-E Tyrrhenian transect from Sardinia to Campania margins (central Mediterranean)*. Tectonophysics, **383**, 171- 192.

Sau A., Lecca L., Lonis R., Secchi F. and Fercia M.L. (2005) - *La seconda fase del Rift Sardo: vulcanismo ed evoluzione dei sub-bacini di Ardara-Chilivani e Bonorva (Sardegna settentrionale)*. Boll. Soc. Geol. It., **124**, 3-20.

Savelli C., Beccaluva L., Deriu M., Macciotta G. and Maccioni L. (1979) - *K/Ar geochronology and evolution of the Tertiary "calc-alkalic" volcanism of Sardinia (Italy)*. J. Volcanol. Geotherm. Res., **5**, 257-269.

Secchi F.A., Brotzu P. and Callegari E. (1991) - *The Arburese igneous complex (SW Sardinia, Italy) - an example of dominant igneous fractionation leading to peraluminous cordierite-bearing leucogranites as residual melts*. Chem. Geol., **92**, 213-249.

Sisson T.W. and Grove T.L. (1993a) - *Experimental investigations of the role of H_2O in calc-alkaline differentiation and subduction zone magmatism*. Contrib. Mineral. Petrol., **113**, 143-166.

Sisson T.W. and Grove T.L. (1993b) - *Temperatures and H_2O contents of low-MgO high-alumina basalts.* Contrib. Mineral. Petrol., **113**, 167-184.

Stormer J.C. and Nicholls J. (1978) - *XLFRAC: A program for the interactive testing of magmatic differentiation models.* Computers & Geosciences. **4**, 143-159.

Sun S.S. and Mc Donough W.F. (1989) - *Chemical and isotopic systematics of oceanic basalts: implications for mantle composition and processes*. In: Saunders A.D. and Norry M.J. (Eds.), Magmatism in the Ocean Basins. Geol. Soc. Lond. Spec. Publ., **42**, 313-346.

Ulmer P. (2007) - *Differentiation of mantle-derived calc-alkaline magmas at mid to lower crustal levels: experimental and petrologic constraints*. Per. Mineral., **76**, 309-325.